

Mesospheric non-migrating tides generated with planetary waves: I. Characteristics

H.G. Mayr^{a,*}, J.G. Mengel^b, E.R. Talaat^c, H.S. Porter^d, K.L. Chan^e

^aGoddard Space Flight Center, Greenbelt, MD 20771, USA

^bScience Systems & Applications, Inc., Lanham, MD, USA

^cApplied Physics Laboratory, Johns Hopkins University, Laurel, MD, USA

^dFurman University, Greenville, SC, USA

^eHong Kong University of Science and Technology, Hong Kong, China

Received 30 September 2003; received in revised form 1 March 2005; accepted 15 March 2005

Available online 20 June 2005

Abstract

In light of the measurements from the TIMED spacecraft and coordinated ground-based observations, we discuss results from a modeling study with our Numerical Spectral Model (NSM), which specifically deals with the non-migrating tides generated in the mesosphere. The NSM extends from the ground to the thermosphere, incorporates Hines' Doppler Spread Parameterization for small-scale gravity waves (GWs), and it describes the major dynamical features of the atmosphere including the wave driven equatorial oscillations (QBO and SAO), and the seasonal variations of tides and planetary waves (PWs). Accounting solely for the excitation sources of the solar migrating tides, the NSM generates through nonlinear interactions also non-migrating tides in the mesosphere that are comparable in magnitude to those observed. (The important non-migrating tides generated explicitly by processes like tropospheric latent heat release and convection are not included.) Large non-migrating tides are produced in the diurnal and semi-diurnal oscillations for the zonal mean (wave number $m = 0$) and in the semidiurnal oscillation for $m = 1$. In general, significant eastward and westward propagating tides are generated for all the zonal wave numbers $m = 1-4$. To identify the cause, the NSM is run without the solar heating for the zonal mean ($m = 0$), and the amplitudes of the resulting non-migrating tides are then negligibly small. In this case, the PWs generated by instabilities are artificially suppressed. This leads to the conclusion that the non-migrating tides are produced through nonlinear interactions between PWs and migrating tides, as had been previously proposed. In the accompanying paper, we present results from numerical experiments, which demonstrate that GW filtering contributes significantly to produce the nonlinear coupling that is involved.

Published by Elsevier Ltd.

Keywords: Non-migrating tides; Gravity waves; Mesosphere dynamics; Numerical modeling

1. Introduction

Satellite measurements with the UARS spacecraft (e.g., Hays et al., 1993, 1994; Shepherd et al., 1993;

McLandress et al., 1996; Burrage et al., 1995a, b; Huang and Reber, 2003) and ground-based observations (e.g., Avery et al., 1989; Manson et al., 1989; Vincent et al., 1989; Jacobi et al., 1999) have shown that the diurnal tides in the mesosphere and lower thermosphere exhibit large seasonal variations, which are modulated by planetary waves (PWs) (e.g., Forbes, 1995; Fritts,

*Corresponding author. Fax: +1 301 286 2323.

E-mail address: hmayr@pop900.gsfc.nasa.gov (H.G. Mayr).

1995a, b). The fundamental diurnal tide exhibits large amplitude maxima during equinox that have been attributed in part to variations in eddy viscosity (e.g., Geller et al., 1997; Yudin et al., 1997; Akmaev, 2001a) and to gravity wave (GW) momentum deposition (Mayr et al., 2001a). Apart from the thermal excitation sources, it is well established from classical tidal theory that the mean zonal circulation affects through advection the seasonal variations of the tides. The above observations and modeling results refer mainly to the dominant westward migrating (or sun-synchronous) tides discussed in textbooks (e.g., Chapman and Lindzen, 1970; Volland, 1988), i.e., the westward propagating diurnal and semidiurnal oscillations with zonal wave numbers $m = 1$ and 2, respectively.

Non-migrating tides (i.e., waves that do not migrate westward with the Sun) are also important in the upper mesosphere. Based on an analysis of UARS High Resolution Doppler Imager (HRDI) measurements over a period of 4 years, Talaat and Lieberman (1999) observed in the diurnal (24 h) tide above 80 km large amplitudes at zonal wave number $m = 0$ and non-migrating components at $m = 1–3$ that equal or exceed those of the migrating tide during some seasons. Forbes et al. (2003a, b) analyzed UARS wind measurements with HRDI and WINDII (Wind Imaging Interferometer) and compared the inferred non-migrating diurnal tides, having zonal wave numbers $m = 0, 1, 2$ and 3, with GCM simulations (Miyahara et al., 1993, 1999; Miyahara and Miyoshi, 1997) and with results from the Global Scale Wave Model (Hagan and Forbes, 2002). Temperature measurements with the Cryogenic Infrared Spectrometers and Telescopes for the Atmosphere (CRISTA) experiment on the Space Shuttle produced significant non-migrating diurnal tides at altitudes between 40 and 90 km (Oberheide et al., 2002). Longitudinal variations more complex than that of $m = 2$ in the migrating semidiurnal tide have been observed in both satellite and ground-based data (e.g., Forbes 1995; Jacobi et al., 1999; Pancheva et al., 2002; Manson et al., 2002). With an empirical model for the HRDI wind measurements on UARS, Huang and Reber (2004) described the seasonal variations of the non-migrating diurnal and semidiurnal tides observed in the upper mesosphere. Hagan and Forbes (2003) have shown that in the troposphere non-migrating semidiurnal tides are generated by large-scale latent heat release associated with tropical convection. Their model simulations demonstrated that this source contributes significantly to the tidal amplitudes in the upper mesosphere and thermosphere.

From satellite data, the inferred phase structure of the non-migrating diurnal tides generally suggests that they propagate upward (Lieberman, 1991; Talaat and Lieberman, 1999). However, the forcing of these tides—due to absorption of solar radiation in tropospheric water

vapor and stratospheric ozone (the main sources for migrating tides), and latent heat release as well as convective or sensible heating—underestimates the observed amplitudes (e.g., Miyahara et al., 1993; Hagan et al., 1997). As an alternative means of generating non-migrating tides, Walterscheid et al. (1986) suggested that GW interactions with migrating tides could be important. Teitelbaum and Vial (1991) proposed nonlinear interactions between migrating tides and PWs; and the observed strong correlations between migrating diurnal and semidiurnal amplitudes and PW activity indicates that this is an important mechanism (e.g., Pancheva et al., 2002; Forbes et al., 1995; Talaat and Lieberman, 1999). Coll and Forbes (2002) demonstrated that nonlinear interactions between the solar driven migrating semidiurnal tide and quasi-stationary $m = 1$ PWs could explain the westward propagating 12-h wave observed in radar measurements near the South Pole (Forbes et al., 1995). In the Kyushu GCM, Miyahara et al. (1999) found that nonlinear interactions between waves could generate the non-migrating tides. Based on simulations with the TIME-GCM model, Hagan and Roble (2001) suggested that nonlinear interactions between the migrating diurnal tide and $m = 1$ PWs could produce non-migrating tides in the upper mesosphere.

We recently demonstrated that the PW mechanism generates in our model $m = 0$ diurnal tides that have amplitudes comparable to those observed in the mesosphere (Mayr et al., 2003). The purpose of the present paper is to describe more fully the non-migrating tides and in particular their seasonal variations. The non-migrating tides are solely generated by nonlinear coupling between migrating tides and PWs. Borrowing some words from one of the reviewers of this paper, two global-scale primary waves (PW and migrating tide) generate a set of global-scale secondary waves (non-migrating tides). Our model thus has in common with the mechanism proposed by Teitelbaum and Vial (1991) that the primary waves are effectively multiplied to generate secondary waves, i.e., $S = P_1 * P_2$. However, in addition to the nonlinearities discussed in their paper, all of which are accounted for, our model also describes the nonlinear interactions associated with GW processes.

GW processes are of central importance for the dynamics of the mesosphere where the tides and PWs attain large amplitudes. In the accompanying paper (Mayr et al., 2005), we present the results of numerical experiments, which indicate that the GWs contribute significantly to increase the magnitude of the non-migrating tides. GW filtering apparently causes the migrating tides and PWs to interact in a nonlinear way. This GW induced nonlinear process is fundamentally different from the conventional fluid dynamical nonlinearities, and this is bound to affect also the dynamical properties of the non-migrating tides that are generated.

2. Numerical spectral model

The design of the NSM was introduced by Chan et al. (1994a), and 2D as well as 3D versions of the model were employed to study the dynamical features of the middle atmosphere (e.g., Mengel et al., 1995; Mayr et al., 1997, 2001a).

The NSM is nonlinear, time dependent, and it is formulated with vector spherical harmonics. The model thus delineates the dynamical components in terms of zonal wavenumbers, m . This yields for the zonal mean ($m = 0$), the seasonal variations (Annual Oscillation, AO; Semi-annual Oscillation, SAO), and the Quasi-biennial Oscillation (QBO); and for $m = 1-4$, the propagating tides and PWs.

In the NSM, the nonlinear Navier Stokes equations are solved to describe the variations around the global mean of temperature and density, covering the atmosphere from the ground up to 400 km (240 km in the present application to speed up computation). The vertical step size for integration is about 0.5 km (below 120 km) and the time step is about 5 min. Marching in time, the state variables are derived for the spherical harmonics and then synthesized to produce solutions. The nonlinear terms and the nonlinear GW parameterization are evaluated in physical space.

Apart from GWs, the NSM is driven: (1) by solar heating for the zonal mean ($m = 0$) component due to UV radiation in the mesosphere and stratosphere taken from Strobel (1978), and due to EUV radiation to describe the thermosphere, and (2) by the heating rates in the middle atmosphere and troposphere, taken from Forbes and Garrett (1978), to generate the migrating solar tides (diurnal and semi-diurnal). The radiative loss in the model is described in terms of Newtonian cooling, which was originally taken from Wehrbein and Leovy (1982). More recently, we have incorporated into our model the cooling parameterization of Zhu (1989).

The PWs that appear in the present version of the NSM are discussed specifically by Mayr et al. (2004a). In the model, no explicit PW source of any kind is prescribed either through convection or topography. The waves are solely excited internally by instabilities, and the baroclinic instability was identified. Plumb (1983) had proposed this mechanism for generating the 2-day wave, and Chan et al. (1994b) proposed that it produced the 4-day wave in their model.

The 3D version of the NSM discussed here differs from earlier versions in that tropospheric heating in the zonal mean ($m = 0$) is applied (Held and Hou, 1980; Lindzen and Hou, 1988; Plumb and Hou, 1992) to reproduce, qualitatively, the observed zonal jets near the tropopause and the accompanying latitudinal temperature variations. Following Dunkerton (1997), we earlier applied such a heat source in our 2D version of the NSM

to study its affect on the wave driven equatorial oscillations (QBO, SAO). In 3D, this additional heat source for $m = 0$ produces through instabilities also PWs, which propagate apparently from the troposphere into the mesosphere (Mayr et al., 2004a).

Following Lindzen (1981), it is well established that small-scale GWs are of central importance to the dynamics of the middle atmosphere (Fritts, 1984). To account for GWs, the NSM incorporates the Doppler Spread Parameterization (DSP) formulated by Hines (1997a, b). The theoretical foundation for the DSP was based on a series of earlier papers (e.g., Hines, 1991a, b), and it has been further solidified recently (Hines, 2001, 2002). The DSP deals with a spectrum of waves that interact with each other to produce Doppler spreading. This in turn affects the interaction of the waves with the background flow, which generates in the NSM a number of dynamical features such as the QBO at low latitudes. The DSP has been discussed extensively in the literature and has also been applied successfully in a variety of other global-scale models (e.g., Akmaev, 2001b; Manzini et al., 1997).

The wave-wave and wave-mean-flow interactions in the DSP are parameterized with Φ_1 and Φ_2 , respectively, which are presently chosen in the model from the middle of the ranges recommended for the DSP. The GW source spectrum at the initial height varies like m^s , with $2 > s > 1$. Choosing $s = 1$, we apply a cut-off minimum wave number of about $m_m = (2 \text{ km})^{-1}$ in accordance with the DSP. This cut-off in the GW source spectrum causes the wave momentum source and related eddy diffusivity to level off at altitudes above 90 km.

Assuming that the GW source at the initial height (taken to be 7.5 km) is isotropic, the momentum flux is proportional to $\sigma_h^3 k^*$, where k^* is the characteristic horizontal wave number in the range $(100 \text{ km})^{-1} < k^* < (10 \text{ km})^{-1}$. A value of $k^* = (125 \text{ km})^{-1}$ is chosen, which is outside this range but close to the lower limit recommended for the DSP. For the GW induced horizontal wind variability at the initial height, we have chosen a latitude independent value that produces $\sigma_h \sim 3 \text{ m/s}$ at 20 km. In reality, the wave activity does change with latitude, as shown from observations by Allen and Vincent (1995), who report that σ_h increases at 20 km from about 2 m/s at mid latitudes to about 3 m/s at the equator.

The DSP assures conservation of GW momentum and energy, and this requires at each altitude, latitude, and longitude that a system of nonlinear equations be solved involving GW parameters, background winds, and Brunt Vaisala frequency. The equations are solved with Newtonian iteration, and convergence is assured by adjusting the time integration step.

With an adjustable parameterization factor, the DSP also provides the isotropic eddy diffusion rate, K , which is taken to be independent of latitude and season. The

increase of K with height, corresponding to the increasing GW momentum source (per mass), is a natural property of the model and is essential to simulate the QBO and SAO. In the present model, K (in m^2/s) varies exponentially with height from about 0.4 at 20 km to 80 at 80 km, but levels off to become constant at about 150 above 90 km. The height dependence of K proves to be important for the tides and PWs in the mesosphere. The GW generated heating rates are not accounted for in the model.

3. Diurnal tides

It is well established that the diurnal tide in the mesosphere is dominated by the propagating mode that peaks at low latitudes (e.g., Chapman and Lindzen, 1970; Volland, 1988). We then show with Fig. 1, during a short period in September, a contour plot of the computed meridional wind oscillations for different zonal wave numbers at 18° latitude (Gaussian point). Generated by the classical migrating solar excitation

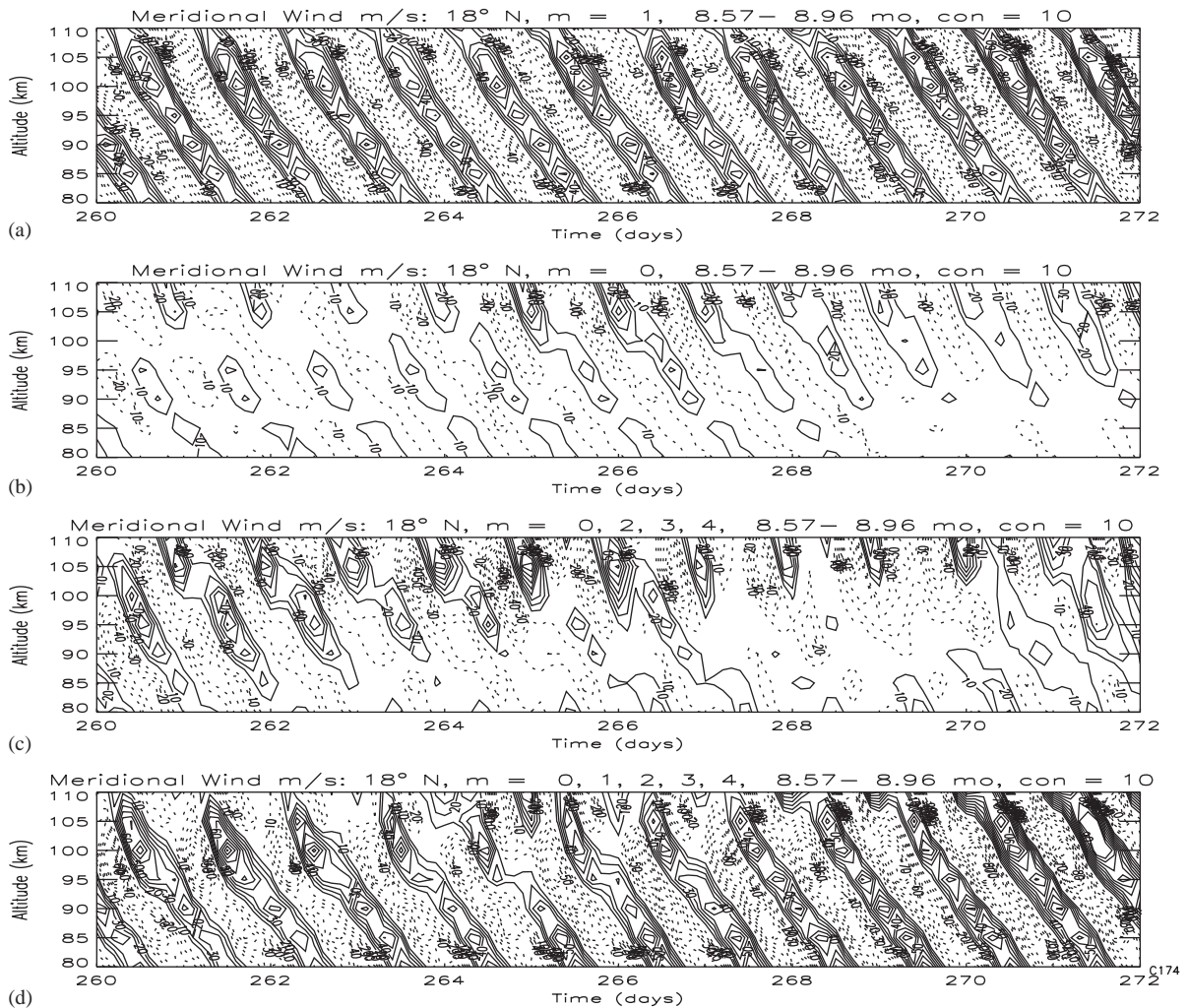


Fig. 1. Plots with constant contour interval of 10 m/s and maximum wind speed of 100 m/s show computed temporal variations of meridional winds at 18° latitude for a short period in September near equinox: (a) for $m = 1$ that includes the dominant westward migrating diurnal tide (period of 1 day), (b) for $m = 0$, (c) for the sum $m = 0, 2, 3, 4$, which does not include the dominant westward migrating $m = 1$ diurnal tide, and (d) for $m = 0, 1, 2, 3, 4$, which contains all the wave numbers retained in the model. (Since the model results are recorded in 5 km intervals, the contours appear ragged.) No filtering has been applied so that, besides the tides, planetary waves are also included. In all four panels, the diurnal tide dominates. The differences clearly reveal that the non-migrating tides, exclusively present in (b) and (c), are also relatively large. The model presented here accounts for the classical westward migrating excitation sources only. The non-migrating tides are solely generated by dynamical interactions that produce nonlinear coupling between the migrating diurnal tide and planetary waves with different zonal wave numbers.

sources, the westward migrating tide is expected to dominate for $m = 1$, and this is seen in Fig. 1a. The shown oscillations, however, also contain the smaller eastward $m = 1$ tide, and any PWs. With identical contour intervals, for comparison, we show in (b) the oscillations for $m = 0$, and in (c) those for $m = 0, 2, 3, 4$ combined, which reveal also diurnal variations although the dominant migrating tide with $m = 1$ is not included. In the latter two cases, the diurnal variations are thus not produced by specified tidal excitation sources of any kind. The variations are solely generated internally through dynamical interactions. With Fig. 1d we then present the computed variations of the total diurnal tide in the model that accounts for $m = 0-4$, and the differences are relatively large when compared with Fig. 1a, where the oscillations are dominated by the migrating $m = 1$ tide.

To provide a broad overview of the diurnal tides generated in the NSM, i.e., migrating and non-migrating, we present in Fig. 2A the computed amplitudes for the meridional winds with a period of 1 day for zonal wave numbers $m = 0-3$, delineating the eastward (solid lines) and westward (dashed lines) propagating components. The tidal oscillations were extracted from a time span of 2 months (24–26 months, January and February) leading into the third model year, with the Sun in the southern hemisphere (years begin at December solstice). For a running window of 10 days, a Fourier analysis was carried out, and the largest amplitudes are plotted versus altitude. To reveal more clearly the amplitude patterns, the lowest 40% of contours are suppressed. The maximum values of the eastward and westward components are stated in the lower left corner of each panel.

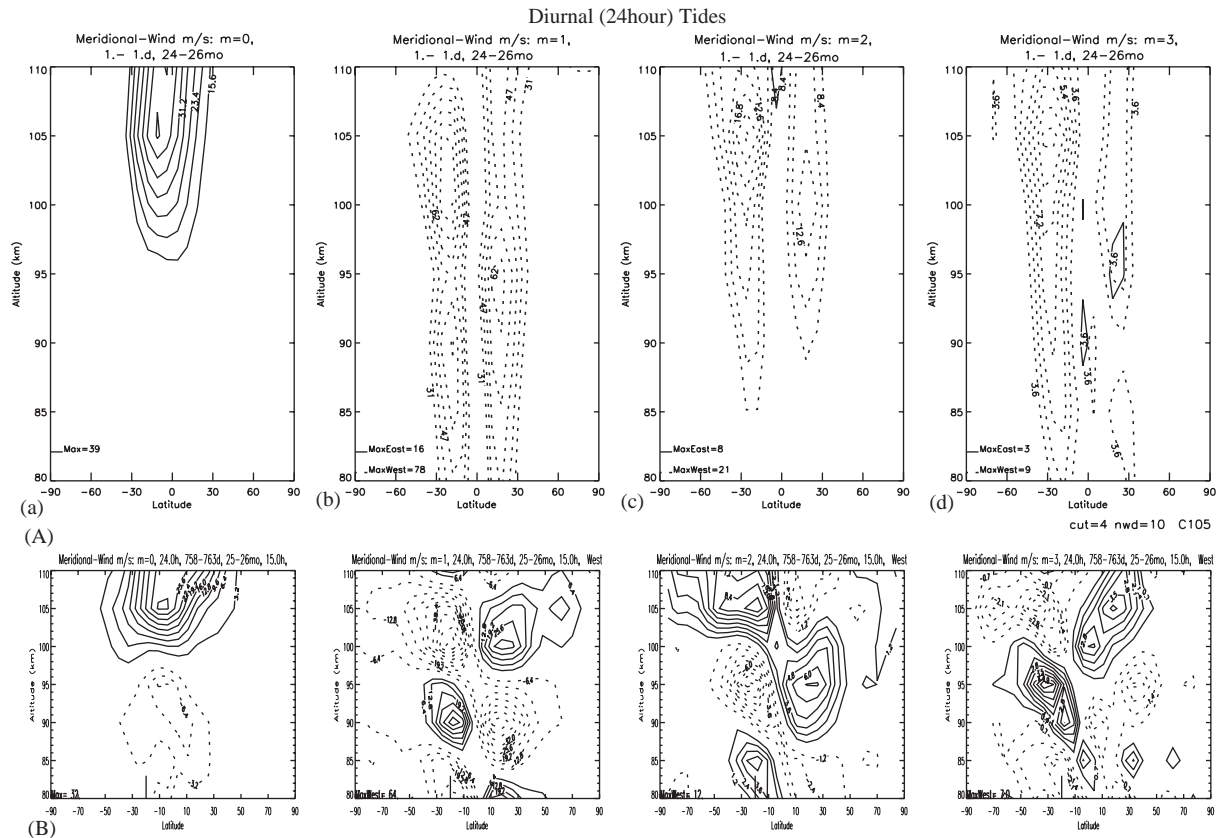


Fig. 2. (A) For a period after solstice (24–26 months or January and February of the third model year), with the Sun in the southern hemisphere, we show for $m = 0-3$ the maximum meridional wind amplitudes of the fundamental diurnal tide (period of 1 day), which are computed from a running window of 10 days. The eastward and westward propagating components are respectively identified with solid and dashed contour lines. The contours are truncated below 40% of the maximum amplitudes to eliminate clutter, but the maximum amplitudes are stated in each panel for both the eastward and westward propagating components. (B) To identify the phase relationships between hemispheres, snapshots of wave oscillations are presented in separate panels for the standing tide ($m = 0$) and the westward migrating tides, which are computed from a period of 5 days during the month 25, in late January.

To reveal the phase relations, we present in Fig. 2B (for each wave number) snap shots for the westward propagating tidal amplitudes of the meridional winds inferred from a 5-day window at the beginning of month 25 near December solstice. Except for $m = 0$, the tides are shown to be hemispherically symmetric, i.e., with the meridional winds having opposite directions in the two hemispheres.

The computed wind amplitudes in Fig. 2 show, as expected, that the westward propagating component dominates for wave number $m = 1$ (with a maximum value of 78 m/s that develops near the time of 26 months, closer to equinox). This tide peaks at low latitudes, and there are significant differences between the northern and southern hemispheres. By comparison, the eastward propagating component (16 m/s maximum) is small and does not appear at the chosen contour intervals. As pointed out earlier, this eastward propagating tide is not generated in the model explicitly by a prescribed source but through nonlinear coupling between the migrating diurnal tide and PWs; and the same is true for all the other tidal components in Fig. 2 including the one for $m = 0$ (39 m/s maximum) that does not propagate zonally. For the zonal wind amplitudes (somewhat smaller and not shown) the relative differences between wave numbers are similar to those for the meridional winds. With the horizontal Coriolis force vanishing at the equator, however, the computed zonal winds for $m = 0$ essentially vanish there. (The smaller vertical Coriolis force is accounted for in the NSM.) The latitudinal structures of the $m = 0$ and eastward diurnal tidal components are consistent with the horizontal winds observed by the UARS/HRDI instrument (Talaat and Lieberman, 1999).

The seasonal variations of the dominant tidal components for $m = 1$ are presented in Fig. 3, where we show the computed meridional wind amplitudes at 100 km during the first two model years, delineating the westward (a) and eastward (b) components. This reveals the characteristic semiannual variation with maxima near equinox, which requires some time to fully develop. As was evident in our earlier model results (Mayr et al., 2001a) for the total $m = 1$ diurnal tide, the large amplitude modulations are a signature of PW interactions. This PW modulation is more effective in modulating the weaker eastward propagating component (b), which is generated apparently by $m = 2$ PWs interacting with the migrating tide. For comparison, we show in Figs. 3c and d the westward and eastward migrating diurnal tides obtained from a solution without the background zonal winds (and temperature variations) for $m = 0$. The migrating tides (c) then are comparable in magnitude to those obtained with the standard model (a). But the eastward tide (d) in this case is much weaker than that from the standard solution (b),

and the reason for this, at least partially, will become clear in the following.

Addressing the relatively large $m = 0$ tide generated in the NSM (Fig. 2Aa), we present in Fig. 4a the amplitude modulations (computed with a 3 day window) at 100 km for the two model years commensurate with Fig. 3. This reveals temporal variations in particular during the first year that resemble those for the $m = 1$ eastward propagating tide (Fig. 3b). After the initial increase that produces a peak around 2 months, the amplitude decreases and then grows again to reach large maxima around 7, 9, and 17 months. For comparison, we also present the zonal winds at 100 km for the computed $m = 1$ PWs (b), which have been proposed to produce the $m = 0$ standing tide through nonlinear coupling with the migrating diurnal tide. After the initial 2 months, the PW amplitudes in (b) decrease and then increase again to reach peak values between 6 and 10 months and later between 14 and 20 months—thus mimicking to some extent the variability in the tide (a) to indicate that the PWs are involved in generating it.

That the PWs indeed are the cause for the non-migrating tides is seen from the results of a numerical experiment reproduced in Figs. 4c and d, for which we selectively turned off the solar heating in $m = 0$ (as for Figs. 3c and d) but retained the migrating tidal excitation source. In this case, apparently, instabilities do not develop to generate the PWs, which is seen from the small amplitudes in Figs. 4d after the initial start-up noise (note the differences in the scales relative to Fig. 4b). As a result, the $m = 0$ tide (Fig. 4c) is then also small, especially during the second half of the first model year and beyond that (not shown). Since the PWs in this case are suppressed in general, this can also explain why the eastward propagating tides in Fig. 3d, generated with $m = 2$ PWs, are so small.

To reveal the seasonal variations of the tides, we present in Figs. 5 and 6 for $m = 1$ and 0, respectively, contour plots of the computed zonal and meridional winds at 100 km. The amplitudes for the eastward and westward tides with a period of 1 day are delineated, covering two model years (24–48 months). As expected, the most persistent seasonal variations appear in the westward propagating tides in Figs. 5a and c, with the amplitude maxima occurring around equinox as observed. Consistent with the PW mechanism, the non-migrating eastward tides appear intermittently, as Fig. 3 had shown, and they tend to be largest around equinox but not consistently every year (Fig. 5b and d). This inter-annual variability may be produced by the QBO that is generated in the model. For $m = 0$ (Fig. 6), the zonal winds at low latitudes tend to be larger in winter and around equinox, but the meridional winds do not reveal pronounced seasonal variations. In the non-migrating tides for $m = 1$ and $m = 0$, the meridional

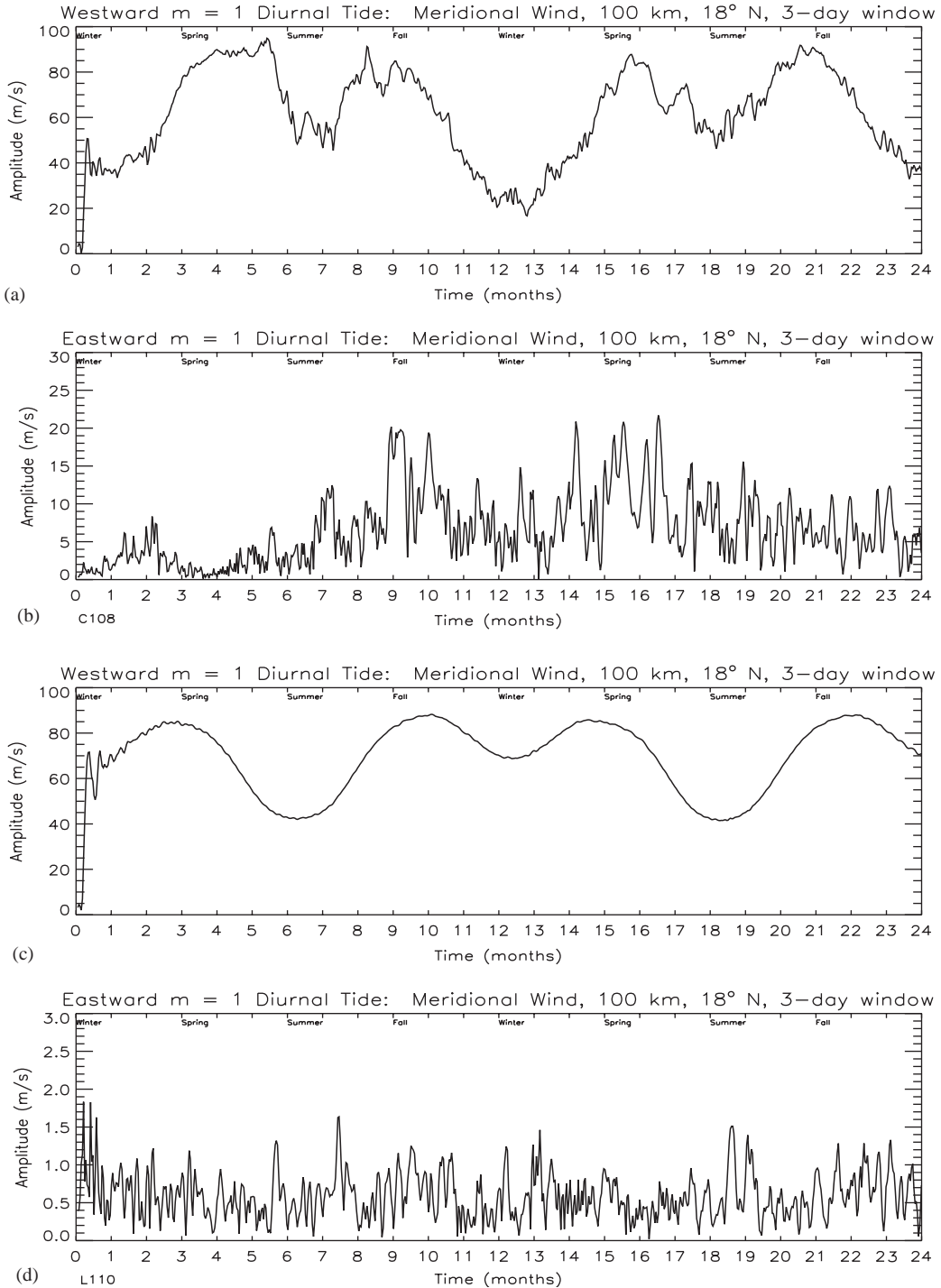


Fig. 3. Computed amplitudes of the zonal wave number $m = 1$ diurnal tide at 100 km altitude for the first two model years, delineating the westward migrating tide (a) and the eastward non-migrating component (b). Note the large planetary wave (PW) modulation of the eastward component (b), which appears also in the combined tidal oscillation (not shown) but is much weaker in the dominant westward component (a). For comparison, the corresponding tidal components (c, d) are shown from a solution obtained without the zonal mean ($m = 0$) circulation and temperature variations. The westward migrating tides (c) generated in this case are comparable in amplitude with those shown in (a), but the eastward component (d) is negligible.

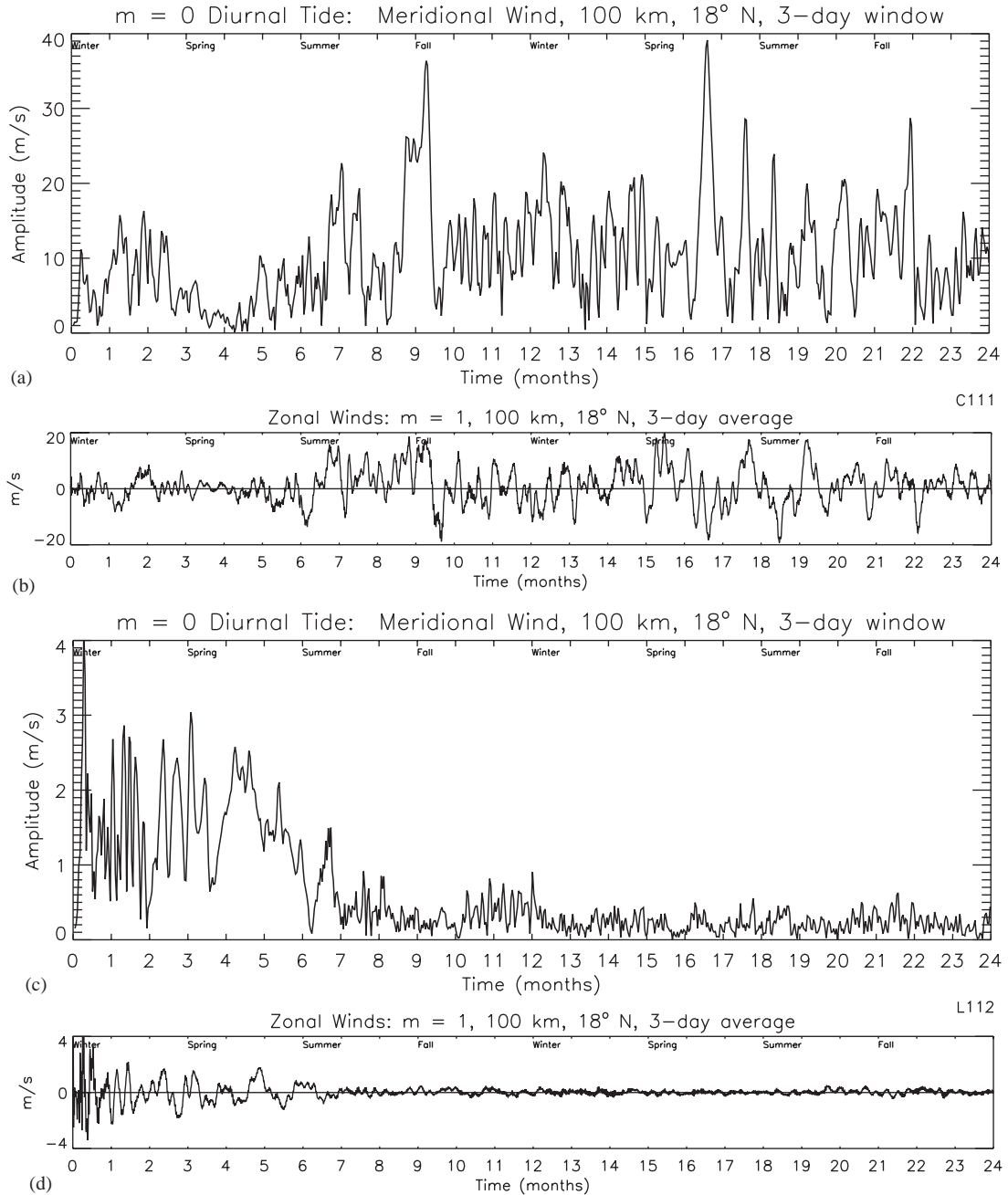


Fig. 4. Temporal variations for the amplitudes of the $m = 0$ tide during the first two model years at 100 km (a), and the computed zonal (c) winds of the $m = 1$ PWs at this altitude. Note the correlations in the temporal variations of the amplitudes for the PWs (b) with the $m = 0$ tide (a) and with the eastward tide in Fig. 3b, in particular during the first model year. Analogous to (a, b), solutions are presented in (c, d) obtained without the $m = 0$ heat source (as for Figs. 3c, 3d). Note the small PW amplitudes (d) for $m = 1$ (with scales different from those in (b)), and the corresponding small $m = 0$ tide (c). After the start-up noise during the first half model year, the PWs and $m = 0$ tide drastically decrease to attain small values that continue to remain small beyond the second model year (not shown). This demonstrates that the $m = 0$ tide is generated in the model through nonlinear interaction between migrating tide and PWs, as Talaat and Lieberman (1999) had proposed.

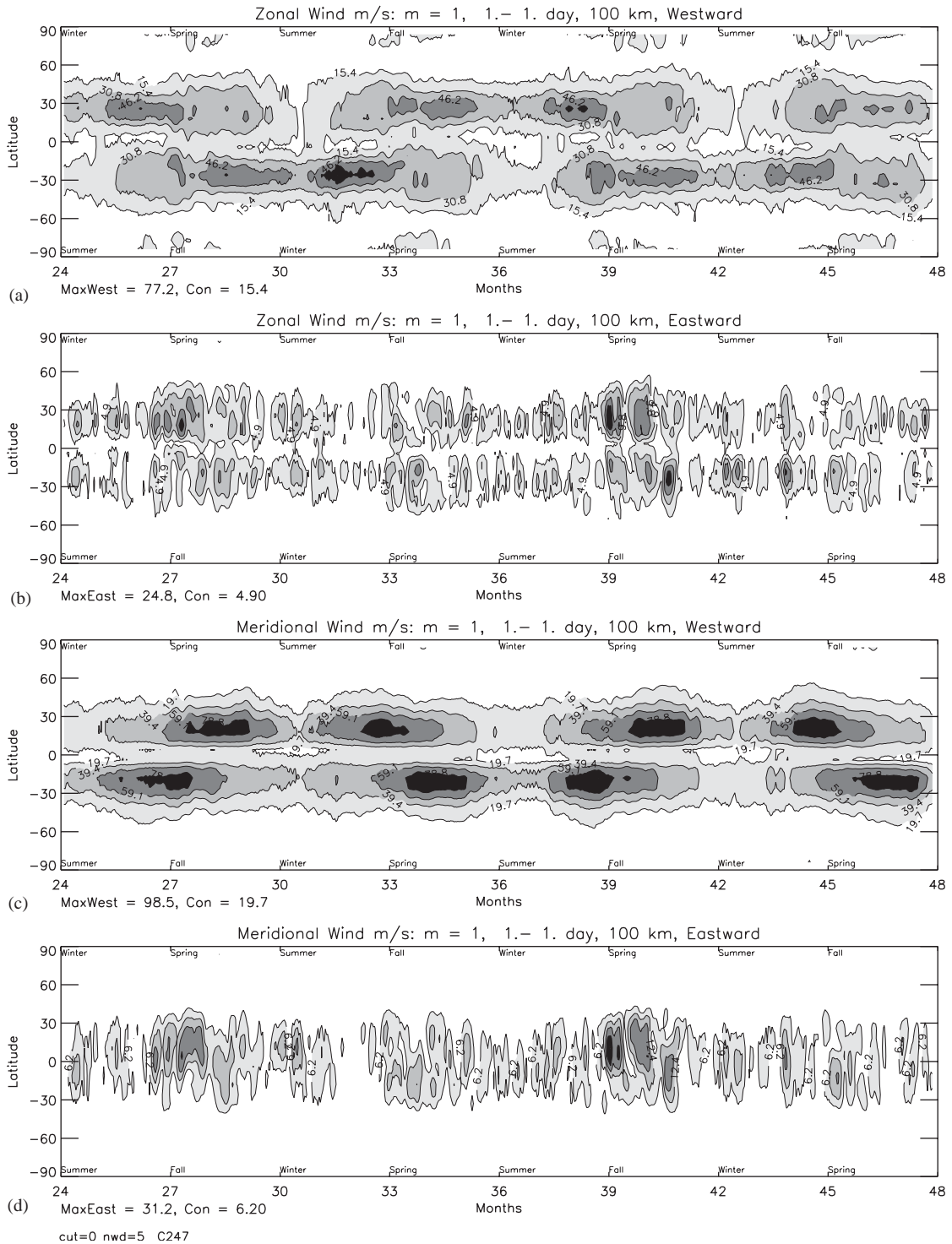


Fig. 5. Seasonal and latitudinal variations of the zonal and meridional winds at 100 km for the $m = 1$ diurnal tide, delineating the eastward and westward components. A running window of 5 days was applied in the analysis. At most, only 5 contour levels are shown, and the maximum amplitudes and contour intervals are stated in the left corner of each panel. As expected, the westward tide (a, c) dominates. While the zonal winds (a) reveal the annual cycle, with amplitude peaks before and after winter solstice, the meridional wind amplitudes (c) peak closer to equinox. The eastward tides (b, d) are small by comparison. The zonal winds (b) peak at low latitudes away from the equator, and the amplitudes tend to be larger around equinox. The meridional winds (d) peak at the equator, and their largest amplitudes tend to occur around equinox.

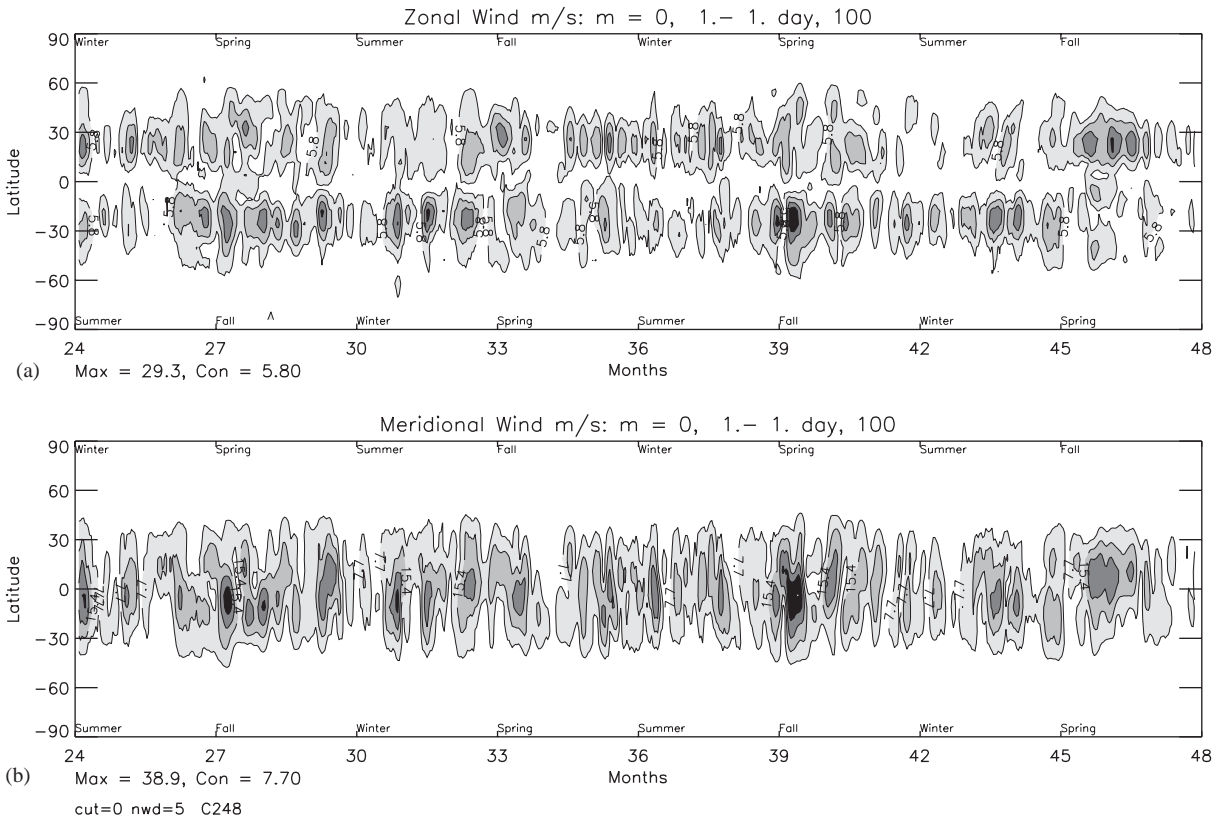


Fig. 6. Similar to Fig. 5 but for the $m = 0$ diurnal tide. It shows that the zonal winds (a) for this component peak at low latitudes coinciding with the dominant westward migrating tide. The tidal activity tends to be reduced during summer. The meridional winds (b) peak at the equator, which is apparent also from Fig. 2a.

winds peak at the equator (Figs. 5d and 6b), and the zonal winds at about 30° latitude (Figs. 5b and 6a), which reflects upon the PWs that are involved. We note that for $m = 1$ eastward propagating Kelvin waves are generated in the model (Mayr et al., 2004a), for which the zonal winds peak at the equator and the periods are between 2 and 3 days.

Corresponding to the zonal and meridional winds shown above, we present in Figs. 7 the seasonal variations of the computed temperature perturbations. For the dominant $m = 1$ westward propagating tide (Fig. 7a), as expected, the amplitudes of the temperature peak at the equator and during equinox. The eastward propagating temperature tide (Fig. 7b) straddles the equator, and the amplitudes tend to be larger around equinox. The temperature oscillations for $m = 0$ (Fig. 7c) are generally also confined to low latitudes and peak away from the equator. These features are qualitatively consistent with the corresponding meridional winds that peak at the equator (Figs. 5d and 6b), which should cause dynamical heating and cooling in the opposing hemispheres away from the equator.

4. Semi-diurnal tides

Analogous to Fig. 2A, we present in Fig. 8A the height and latitude variations of the semi-diurnal tidal amplitudes in the meridional winds for the time span from 24 to 26 months (January and February of third model year). The westward migrating tide at $m = 2$ dominates, but the non-migrating tides at $m = 0$ and $m = 1$ in particular are also large. The tidal components for $m = 3$ and 4 (not shown) are significant as well. In contrast to the diurnal tide that peaks at low latitudes (Fig. 2b), the dominant westward migrating semi-diurnal tide near solstice is anti-symmetric about the equator as seen from the snapshot of the wave oscillation in the lower panel (B) of Fig. 8c (the meridional winds in both hemispheres having the same direction). Commensurate with that, the non-migrating $m = 0$ and 3 components then are also anti-symmetric, as seen from Figs. 8Ba and Bd.

As Fig. 8c shows, the dominant migrating semi-diurnal tide peaks at mid to high latitudes. Analogous to Fig. 3, we then present in Fig. 9 for $m = 2$ the computed

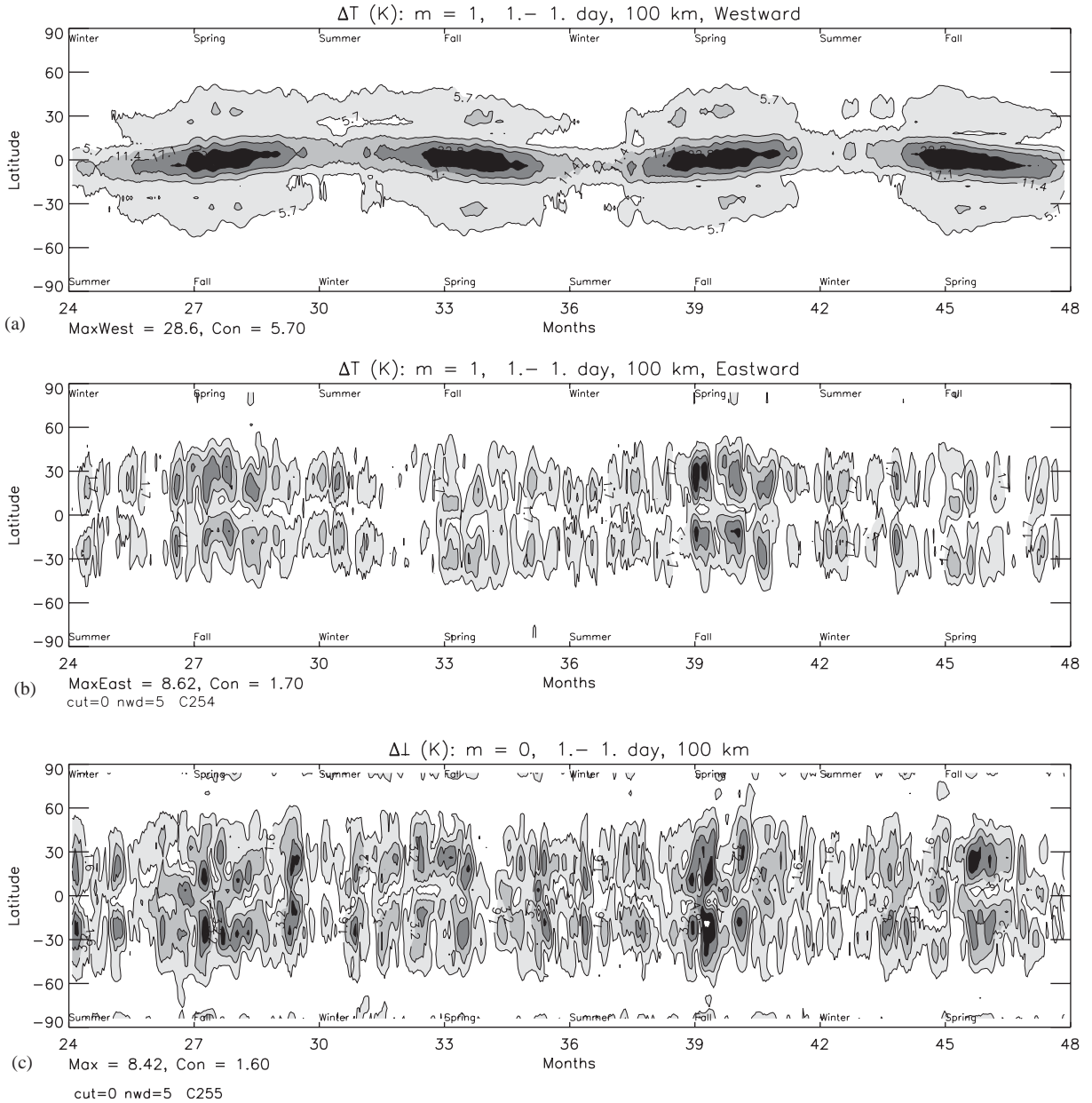


Fig. 7. Similar to Fig. 5, but showing the computed temperature perturbations for the westward (a) and eastward (b) propagating $m = 1$ diurnal tides. As expected, the amplitudes of the dominant westward migrating tide (a) peak at the equator near equinox. For the much weaker eastward component (b), the temperature perturbations occur intermittently and tend to straddle the equator. Computed temperature perturbations (c) for the $m = 0$ diurnal tide. As in (b), the temperatures again straddle the equator, which is consistent with the meridional winds (Fig. 6b) that peak at the equator to cause dynamical heating and cooling in the opposing hemispheres at low latitudes. Maximum values and contour intervals are stated.

meridional wind amplitudes at 100 km for 62° latitude (Gaussian point), delineating again the westward (a) and eastward (b) components. This shows the characteristic seasonal variation with maxima during summer and

winter months. An analysis of earlier model results demonstrated that these variations are in part caused by nonlinear coupling involving the diurnal tide, which was attributed to GW filtering (Mayr et al., 2001a). As is the

Semi-diurnal (12hour) Tides

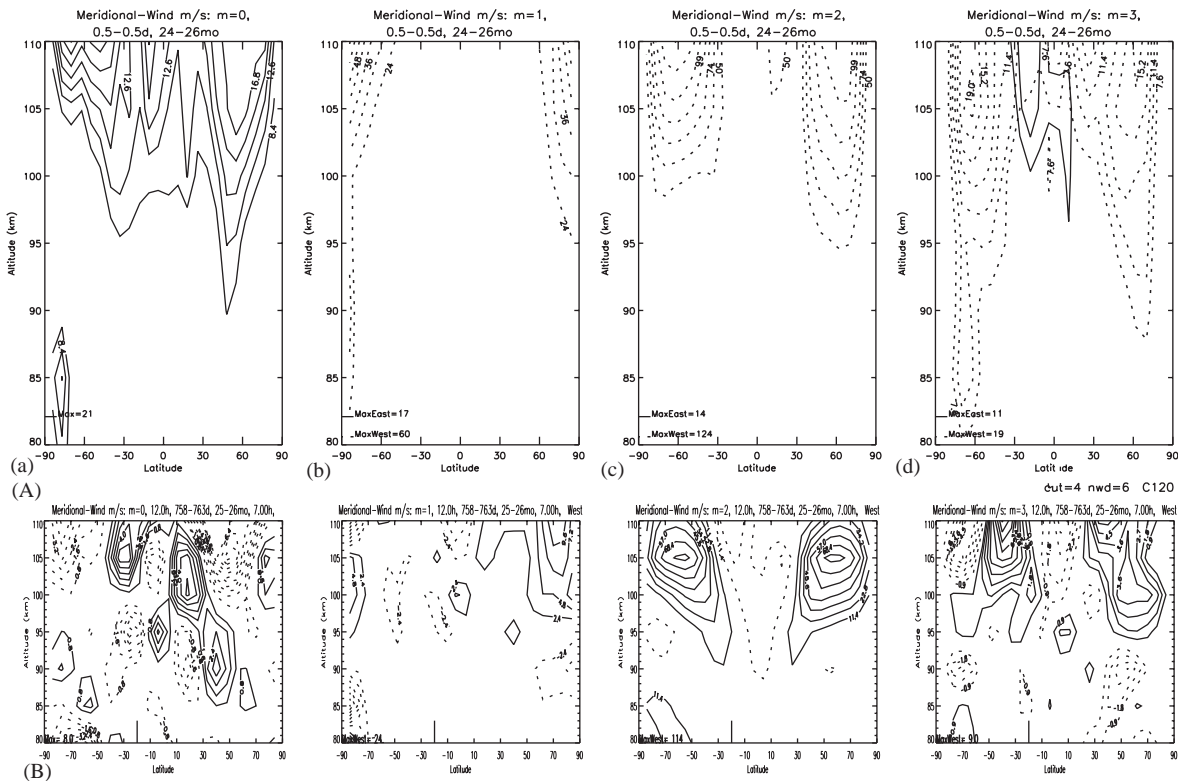


Fig. 8. (A) Analogous to Fig. 2 but for the semi-diurnal tide (12h period). In this case, the dominant westward migrating tide is associated with $m = 2$ (c). Large non-migrating tides are generated for $m = 0$ (a) and $m = 1$ (b) in particular. The contours are truncated below 40% to eliminate clutter, but the maximum amplitudes are stated for the eastward and westward components. (B) Snapshots of the meridional winds for the semi-diurnal winds reveal that they tend to be hemispherically anti-symmetric, i.e., with the same meridional wind directions in the two hemispheres.

case for the diurnal tide (Fig. 3), the amplitude modulations appear to be generated by PW interaction, which is particularly effective for the much weaker eastward propagating component (Fig. 9b). Without the background zonal mean ($m = 0$) heat source, the amplitudes of the westward migrating semi-diurnal tide (c) are comparable in magnitude to those obtained with the zonal circulation. However, the eastward tides (d) are then negligibly small due to the lack of PW excitation.

The $m = 0$ semi-diurnal tide grows in amplitude at least up to 110 km (Fig. 8Aa), consistent with the westward migrating tide (Fig. 8Ac) that is involved to generate it. Analogous to Fig. 4, we present in Fig. 10a, for the first two model years, the seasonal variations of the $m = 0$ semi-diurnal tide at 110 km. During the first year, the variations to some extent resemble those seen in Fig. 4 for the diurnal tide. After the first 2 months, the amplitude decreases

and then grows again to reach a large maximum at around 8 months. In this case, the PWs with $m = 2$ can generate the semidiurnal $m = 0$ tide through nonlinear interaction. For comparison, we thus present the computed $m = 2$ PWs at 110 km for the meridional winds (Fig. 10b). This shows that the temporal variations of the PWs tend to correlate with the patterns in the $m = 0$ tide (a). When we turn off the solar heating for $m = 0$, the PWs (Fig. 10d) virtually disappear, and commensurate with that the $m = 0$ tide is then also small (c).

To describe the seasonal variations, we show in Fig. 11 the computed meridional winds for the $m = 2$ semi-diurnal tide at 100 km. The dominant westward propagating tide (a) exhibits primary and secondary peaks in the winter and summer hemispheres, respectively. Seasonal variations also appear in the eastward propagating tides (b), which develop throughout the year but not in the summer hemisphere.

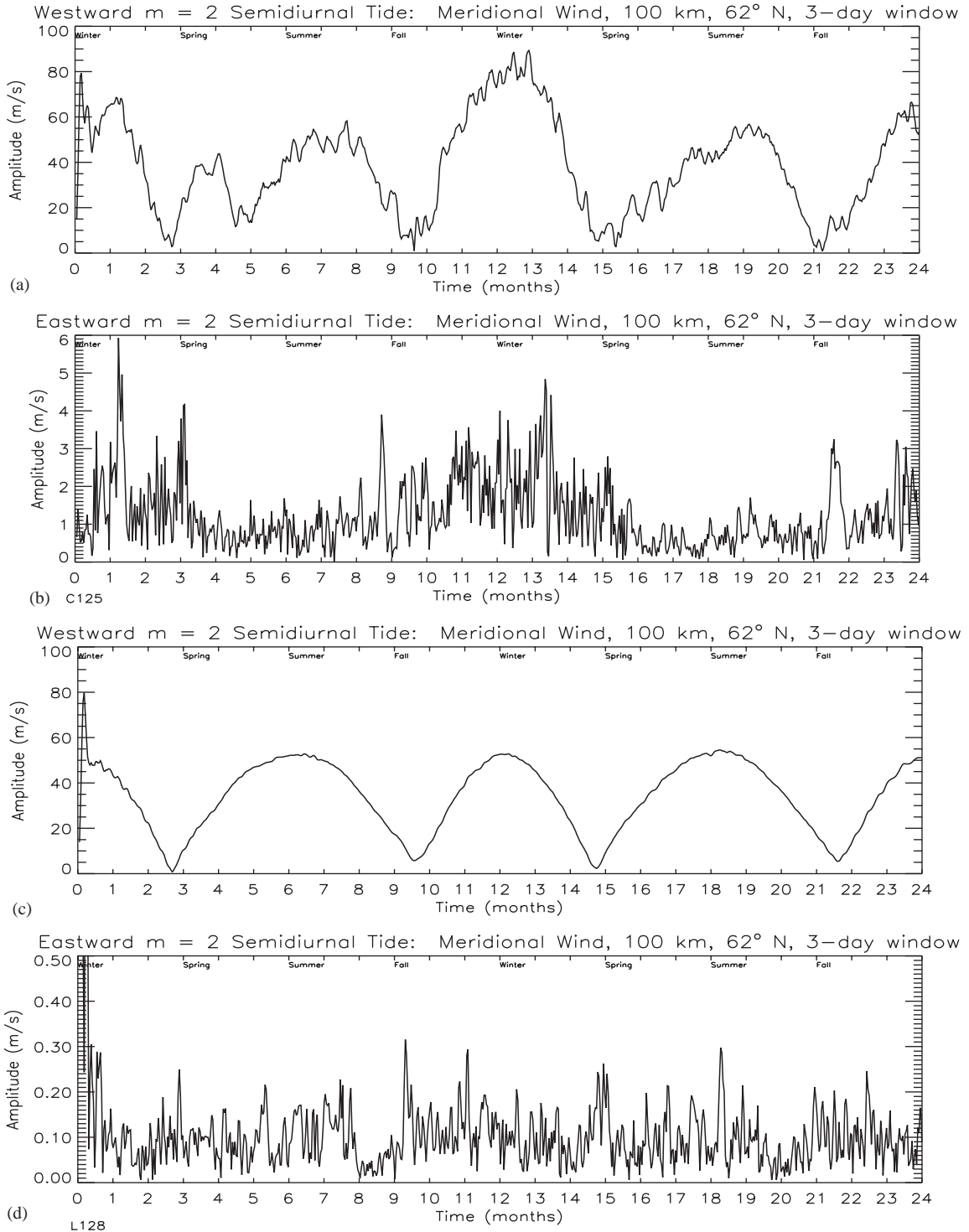


Fig. 9. Analogous to Fig. 3 but for the semi-diurnal tide with $m = 2$ and at 62° latitude. Note the tidal variability of the eastward migrating tide (b), which is largest during winter months at 100 km where the westward migrating tide (a) peaks. Without $m = 0$ heat source, to suppress the PWs, the corresponding westward (c) and eastward (d) tidal components are shown for comparison.

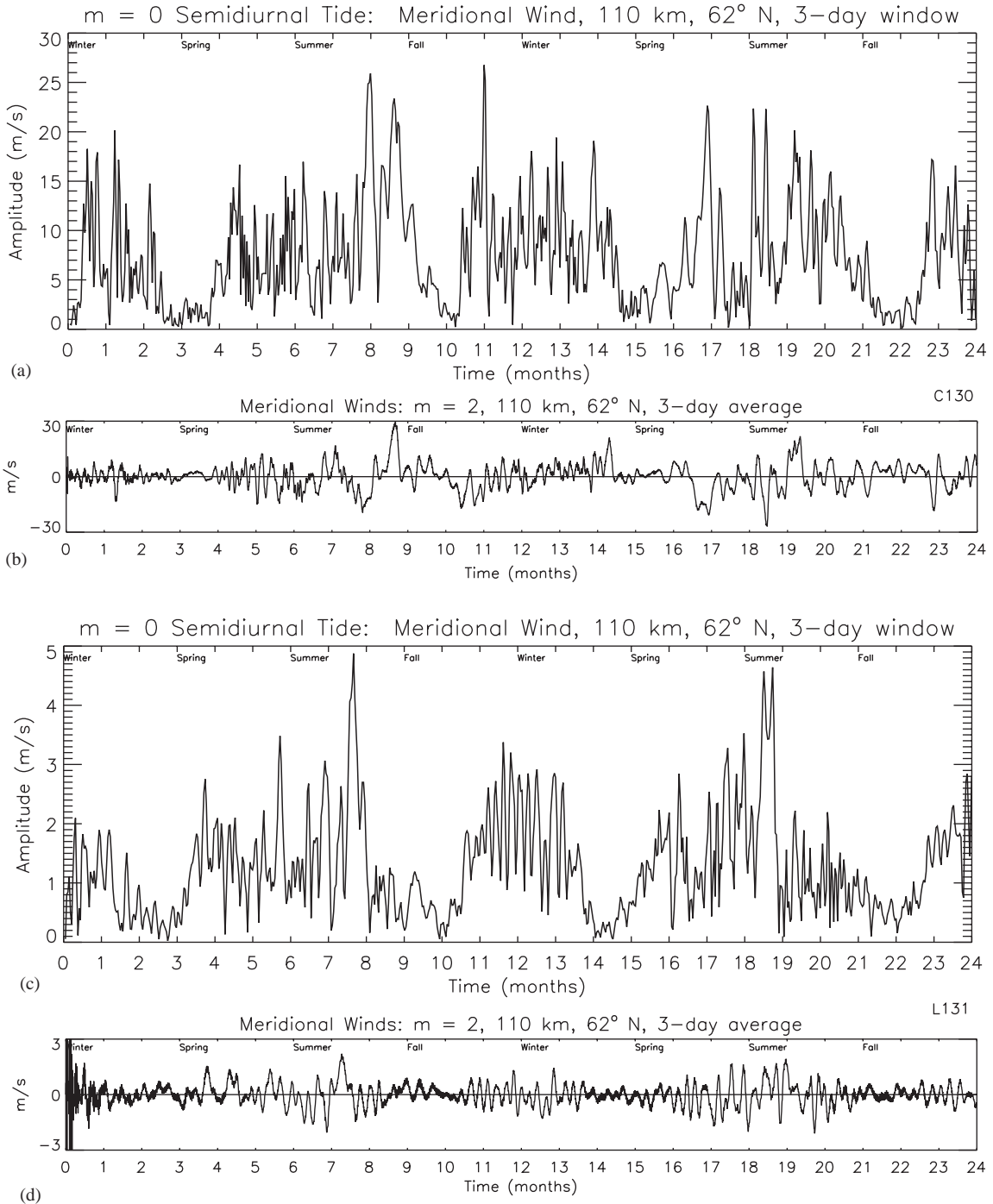


Fig. 10. Analogous to Figs. 4 but for the $m = 0$ semi-diurnal tide (a) and the $m = 2$ PWs (b) at 110 km and 62° latitude, which reveal correlations. For comparison, a solution is presented for the $m = 0$ tide (c) and PWs (d) without the $m = 0$ heat source. This demonstrates again that PWs are involved in generating this non-migrating tide.

Their magnitudes however are much smaller as seen from the numerical values of the maximum amplitudes that are stated in the left bottom corner

of each panel. For $m = 0$ (not shown), the wind amplitudes at 100 km are also larger in the winter hemisphere.

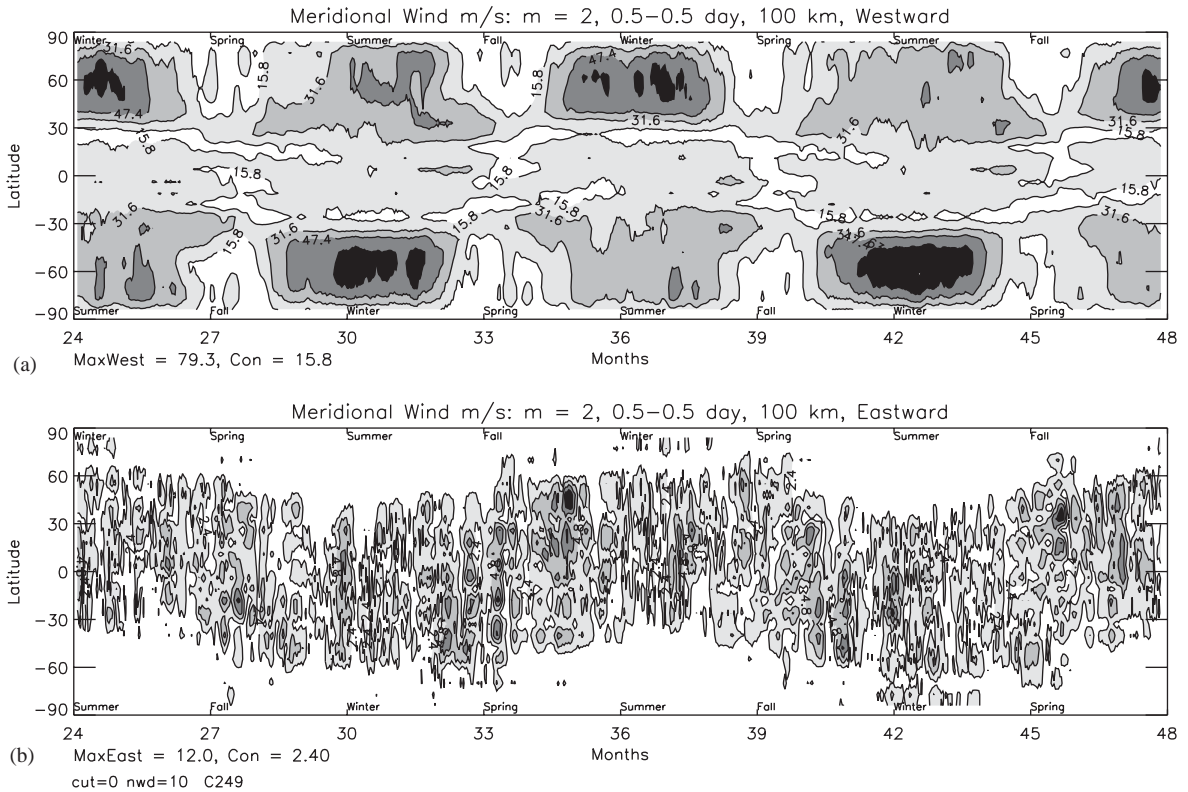


Fig. 11. Analogous to Fig. 5 but for the semi-diurnal tide with $m = 2$. It shows for the westward migrating tide that the meridional winds (a) peak at around 60° latitude, with primary and secondary maxima in winter and summer, respectively. The eastward migrating tides (b) are highly variable and small by comparison. They tend to peak in winter and around equinox and then extend across the equator.

Analogous to Fig. 11, we present with Fig. 12 the corresponding temperature perturbations that reveal systematic seasonal variations. In the dominant westward tide (a), which is anti-symmetric about the equator around solstice, the largest amplitudes occur in the winter hemisphere, but the somewhat weaker peaks in summer occur over longer time span. Consistent with the winds in Fig. 11b, the eastward propagating temperature tides (Fig. 12b) are largest during winter months and around equinox.

As seen in Fig. 11, the dominant westward migrating semi-diurnal tide ($m = 2$) in the upper mesosphere peaks at latitudes around 60° . For obvious geometric reasons, this tide vanishes at the poles, as do all the other oscillations for zonal wave numbers $m \neq 1$. In contrast, oscillations with $m = 1$ are unique in that they do not need to vanish at the poles but instead may attain large amplitudes there. Interactions between the migrating semi-diurnal tide and $m = 1$ PWs thus can become important at high latitudes to produce an $m = 1$ non-migrating semi-diurnal tide, as Forbes et al. (1995) had

proposed. Such tidal oscillations are shown in Fig. 13, where we present contour plots of the computed temporal variations for the meridional winds at high latitudes (77°). With identical contour intervals, the semi-diurnal variations at $m = 1$ (b) are shown to be comparable to those for $m = 2$ (a), which include the dominant westward propagating semi-diurnal tide.

In Fig. 14 we show for 84°N the computed non-migrating $m = 1$ semi-diurnal tide together with the PWs that are involved in generating it. Solutions are presented with (a, b) and without (c, d) the $m = 0$ solar heating. With that source in the standard model, the PWs are strong (b), and they tend to be correlated with the non-migrating tide (a). Without the $m = 0$ source, PWs are essentially not excited as seen in (d), and the $m = 1$ semidiurnal tide (c) is then also small (note the different scales).

The $m = 1$ semidiurnal tides reveal systematic seasonal variations as Fig. 15 shows for the meridional winds. In the westward migrating tides (a), which peak at the poles, the largest amplitudes (exceeding 50 m/s)

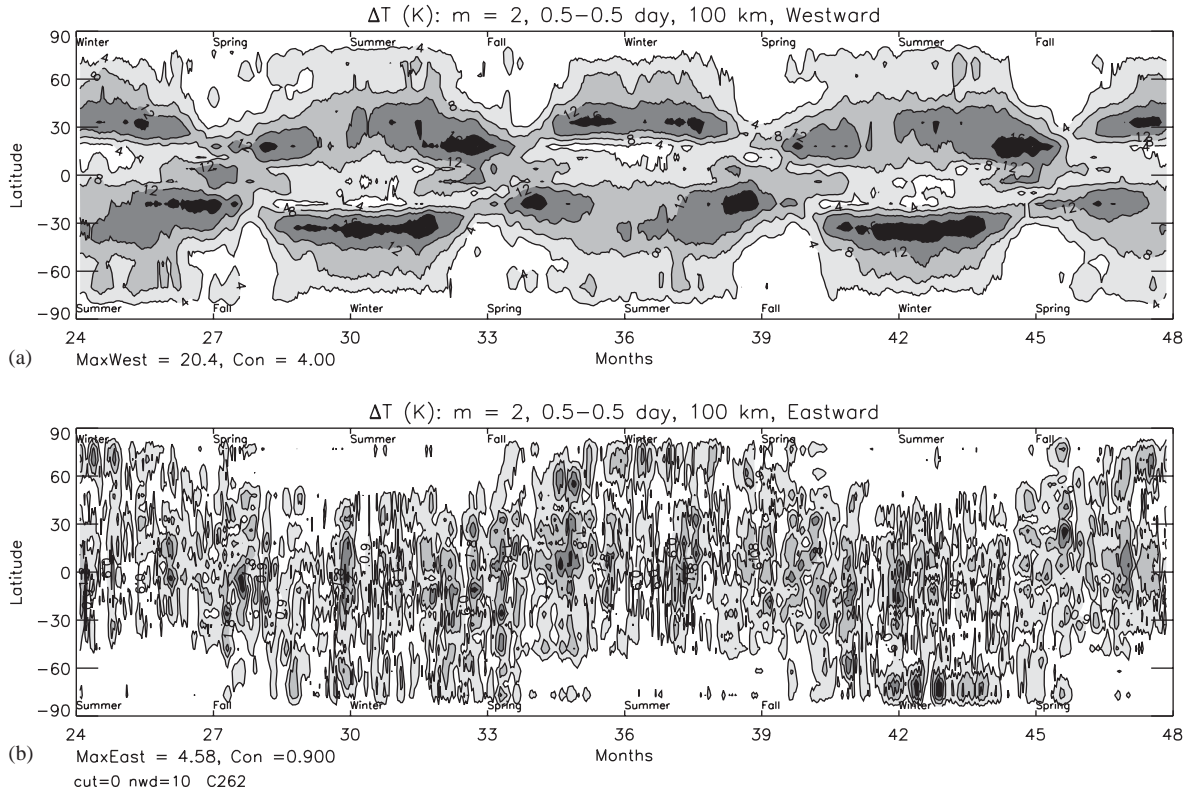


Fig. 12. Analogous to Fig. 7 but for the semi-diurnal tide at $m = 2$. The temperature perturbations of the dominant westward migrating tide (a) peak in winter and reveal a secondary maximum in summer (as in Fig. 11a for the winds). The intermittent eastward propagating tides (b) reveal seasonal variations similar to those seen in the meridional wind oscillations (Fig. 11b).

tend to occur during equinox and occasionally also during winter months. In contrast, the eastward propagating tides (b) are generally confined to latitudes below 70° and they are much weaker (around 10 m/s).

As a signature of solar forcing, our model produces systematic seasonal variations not only in the migrating tides but in the non-migrating diurnal and semi-diurnal tides as well. To provide a more thorough understanding will require that we relate these variations to the seasonal variability of the PWs and migrating tides, which goes beyond the scope of this paper.

5. Discussion and conclusion

We have shown here for the diurnal and semi-diurnal tides, that non-migrating components with relatively large amplitudes appear in the NSM at altitudes above 80 km. The evidence presented demonstrates that these tides are produced by nonlinear dynamical interactions between migrating tides and PWs, and that the latter are

apparently generated in the model through the instabilities that arise in the zonal mean ($m = 0$) circulation associated with temperature and pressure variations. The baroclinic instability was proposed by Plumb (1983) for the 2-day wave and was identified in the present model as a potential PW source (Mayr et al., 2004a), and Chan et al. (1994b) suggested that this instability produced 4-day waves in their model.

The PW mechanism was introduced by Teitelbaum and Vial (1992), and it was specifically invoked by Forbes et al. (1995) to explain the $m = 1$ non-migrating semidiurnal tide at polar latitudes. Nonlinear interactions for example between long period PWs for $m = 1$ and 2, $\exp(i\Omega t \pm im\phi)$, and westward propagating tides, $\exp(im\omega t - im\phi)$, would yield with $\Omega \ll \omega$ approximately $\approx \exp(im\omega t)$, and $\approx \exp(im\omega t - 2im\phi)$, each modulated by the PWs. We have seen from Figs. 4 for the diurnal tide and from Fig. 10 for the semi-diurnal tide that this indeed appears to be the explanation for the NSM. The PW mechanism was also shown to operate for the large $m = 1$ semi-diurnal tide as seen from Fig. 14. A limited inspection of our model results in fact indicates that

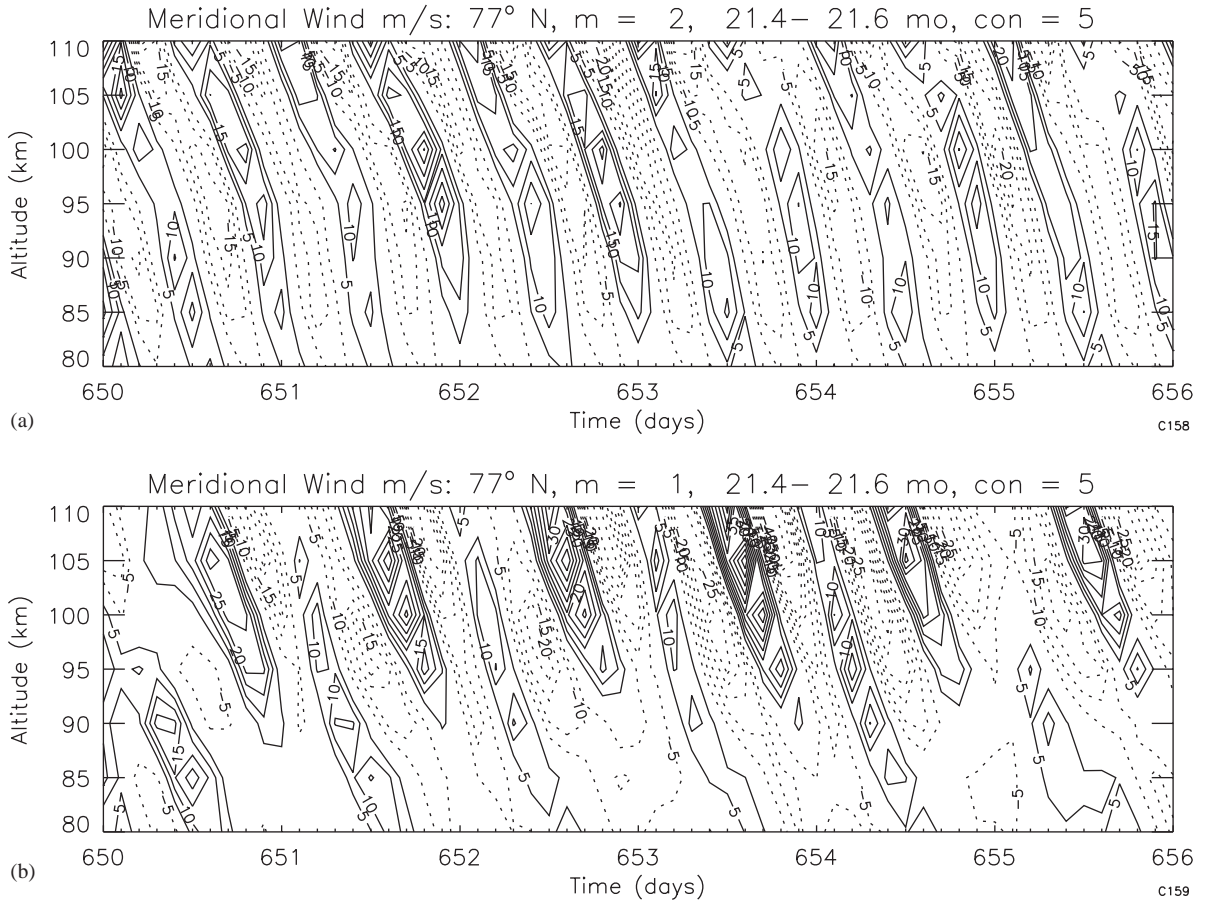


Fig. 13. Analogous to Fig. 1 but with constant contour interval of 5 m/s and maximum wind speed of 50 m/s, the plots show the computed temporal variations of meridional winds at 77° latitude for a period in October of the second model year, (a) for $m = 2$ and (b) for $m = 1$. (Recorded in 5 km intervals, the contours appear ragged.) The dominant westward migrating semi-diurnal tide is associated with $m = 2$ (a). But the 12-h periodicity is also apparent in $m = 1$ (b) where it represents a relatively large non-migrating tide.

PWs are involved in general to generate the non-migrating tides.

The NSM solves the nonlinear Navier Stokes equations and thus accounts for the above-discussed nonlinear coupling. There are a number of nonlinear processes that can be in play such as advection and adiabatic heating, and they still need to be investigated.

Our model also accounts for GW processes and, in particular, for the filtering of GWs, which can produce nonlinear interactions as we had argued earlier. GW filtering is a candidate for generating nonlinear interactions between the QBO and SAO to produce inter-seasonal variations in the upper mesosphere, between the QBO and the AO to produce quasi-decadal oscillations, and between the diurnal tides to generate semidiurnal tides.

In the present case, upward propagating GWs may encounter a PW and amplify it (Mayr et al., 2001b). This amplification occurs at the expense of the GW momentum flux in a particular direction, which in turn decreases the flux in that direction. The GW flux, thus modified by the PW, then encounters the tide and amplifies it (Mayr et al., 2001a). The PW modulation of the GWs is thereby transferred to the tide, which represents a nonlinear interaction. Such a process is likely to be less important at lower altitudes where the filtering would not cut deeply into the momentum flux. But at higher altitudes, this process becomes increasingly more important as the remaining GW momentum flux gets depleted by absorption and by the accompanying filtering. The nonlinear process of GW filtering thus should become increasingly important at higher altitudes. Combined with the

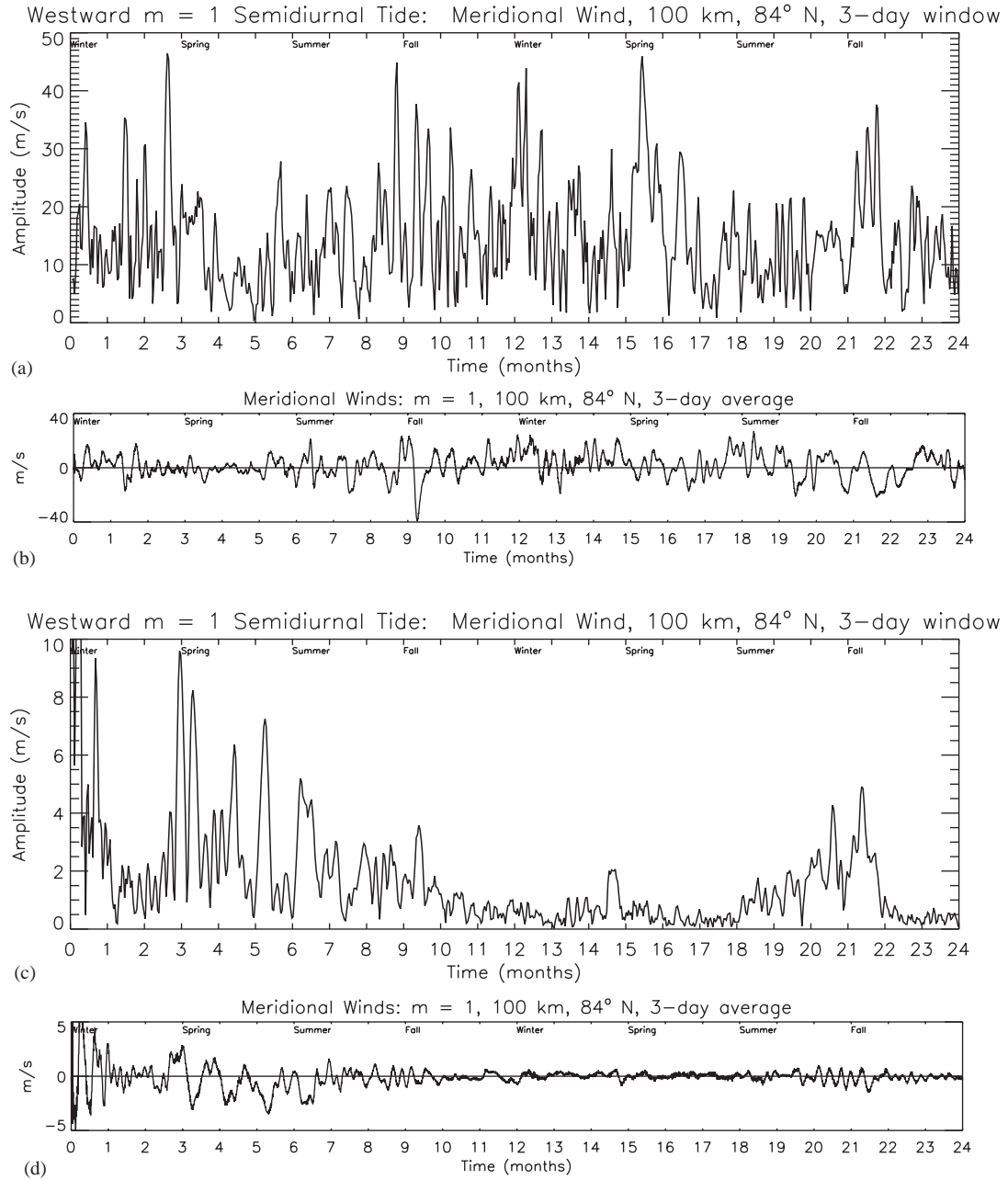


Fig. 14. Temporal variations of amplitudes for the semi-diurnal $m = 1$ meridional winds at 84° N (a), and the PWs for $m = 1$ (b) that are involved in generating this non-migrating tide as Forbes et al. (1995) had proposed. For comparison a solution is shown without $m = 0$ heating, which yields tidal amplitudes (c) and PWs (d) that are small.

fact that the tides and PWs tend to grow with height, this may explain in part why the non-migrating tides become so important in the upper mesosphere and lower thermosphere as our model results indicate.

In conclusion, we present a schematic with Fig. 16 that summarizes the results from our modeling studies and outlines our present understanding of the processes that are involved in generating the non-migrating tides. The NSM is driven by solar heating, which is the source

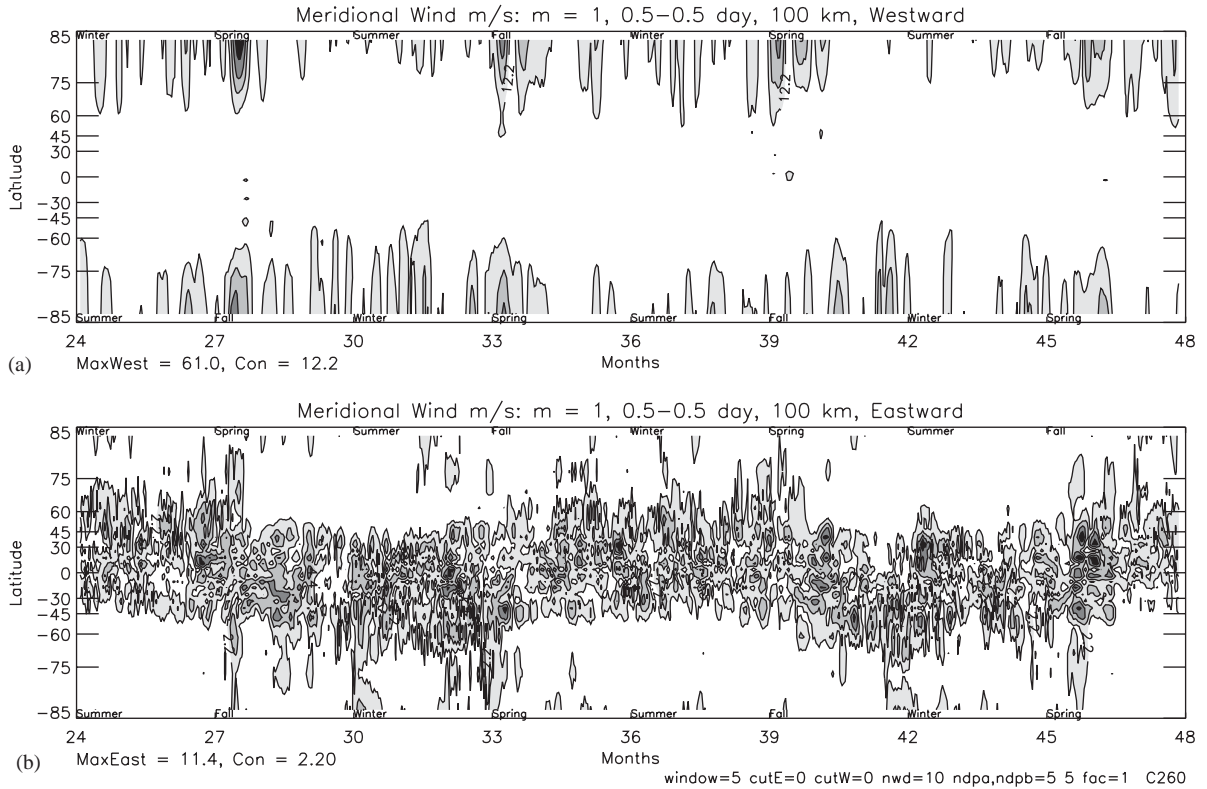


Fig. 15. Analogous to Fig. 11 but showing the seasonal variations of meridional winds for the $m = 1$ non-migrating semi-diurnal tides, westward (a) and eastward (b). The Mercator projection is applied to expand the regions at high latitudes. Note that the westward propagating tide peaks in the polar regions, with amplitudes exceeding 50 m/s, while the much weaker eastward tides tend to be confined to low and mid latitudes. Maximum values and contour intervals are stated.

for (a) the mean zonal circulation and temperature variations and (b) the westward migrating diurnal and semi-diurnal tides. Instabilities associated with the zonal mean generate the PWs, and through advection the mean zonal circulation filters the PWs, and the tides. In addition, a steady source of parameterized small-scale gravity waves (GWs) is imposed in the troposphere, which for simplicity is taken to be independent of latitude and season. As discussed in the literature and is outlined in Fig. 16, the GWs produce temperature and wind reversals in the upper mesosphere (1) and affect significantly the tides (2) and PWs (3). Nonlinear coupling between the migrating tides and PWs then produces the non-migrating tides in the NSM. By artificially turning off the solar heating for the mean zonal circulation, the PWs were suppressed or eliminated and so were the non-migrating tides.

We have argued that GW processes contribute through different channels (items 1–3 in Fig. 16) to the non-migrating tides by influencing their building blocks. Without GWs, the mean zonal circulation would be

significantly different (Lindzen, 1981), which in turn affects the instabilities that generate the PWs. And the migrating tides and PWs are amplified by the GWs. In the accompanying paper (Mayr et al., 2005), we presents the results of numerical experiments, which indicate that the GWs are also important for the process of nonlinear coupling itself that causes the migrating tides and PWs to generate the non-migrating tides (item 5 in Fig. 16).

In a separate paper, Talaat et al. will discuss the non-migrating 12-h pseudo tides in the model, which are associated with the internal planetary-scale inertio GWs (Mayr et al., 2004b) that can be generated without the thermal excitation sources for the solar driven westward migrating tides. Another subject that needs to be discussed will deal with the importance of tropospheric zonally symmetric ($m = 0$) cumulus heating, which produces the zonal jets near the tropopause and is a source of PWs, which in turn contribute significantly to the non-migrating tides in the upper mesosphere.

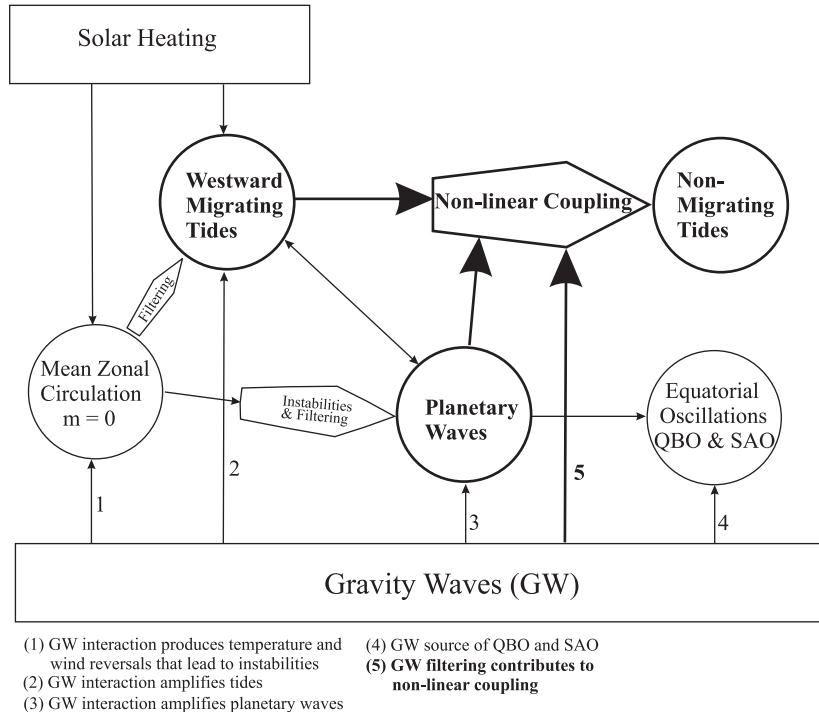


Fig. 16. Schematic to illustrate the dynamical features and processes that produce the non-migrating tides in the present NSM. The model is driven by: (a) solar heating that generates the zonal mean ($m = 0$) circulation and temperature variations, (b) the westward migrating tides, and (c) a gravity wave (GW) source taken for simplicity to be independent of latitude and season. The PWs are generated solely by instabilities, and they are filtered by the mean zonal circulation. Enumerated with items 1–4 and discussed in the literature, the GWs affect: (1) the zonal mean ($m = 0$) circulation (and temperature variations), (2) the migrating tides, (3) the PWs, and (4) the equatorial oscillations (QBO, SAO). GW filtering is important for the nonlinear coupling between migrating tides and PWs to generate non-migrating tides (item 5), and this is discussed in the accompanying paper (Mayr et al., 2005).

Acknowledgments

The authors are indebted to two anonymous reviewers for critical and constructive comments, which greatly contributed to improve the paper.

References

- Akmaev, R.A., 2001a. Simulation of large-scale dynamics in the mesosphere and lower thermosphere with the Doppler-spread parameterization of gravity waves: 2. Eddy mixing and the diurnal tide. *Journal of Geophysical Research* 106, 1205.
- Akmaev, R.A., 2001b. Simulation of large-scale dynamics in the mesosphere and lower thermosphere with the Doppler-spread parameterization of gravity waves: 1. Implementation and zonal mean climatologies. *Journal of Geophysical Research* 106, 1193.
- Allen, S.J., Vincent, S.A., 1995. Gravity wave activity in the lower atmosphere: Seasonal and latitudinal variations. *Journal of Geophysical Research* 100, 1327.
- Avery, S.K., Vincent, R.A., Phillips, A., Manson, A.H., Fraser, G.R., 1989. High latitude tidal behavior in the mesosphere and lower thermosphere. *Journal of Atmospheric and Terrestrial Physics* 51, 595.
- Burrage, M.D., Hagan, M.E., Skinner, W.R., Wu, D.L., Hays, P.B., 1995a. Long-term variability in the solar diurnal tide observed by HRDI and simulated by the GSWM. *Geophysical Research Letters* 22, 2641.
- Burrage, M.D., Wu, D.L., Skinner, W.R., Ortland, D.A., Hays, P.B., 1995b. Latitude and seasonal dependence of the semidiurnal tide observed by the high-resolution Doppler imager. *Journal of Geophysical Research* 100, 11313.
- Chan, K.L., Mayr, H.G., Mengel, J.G., Harris, I., 1994a. A ‘stratified’ spectral model for stable and convective atmospheres. *Journal of Computational Physics* 113, 165.
- Chan, K.L., Mayr, H.G., Mengel, J.G., Harris, I., 1994b. A spectral approach for studying middle and upper atmospheric phenomena. *Journal of Atmospheric and Terrestrial Physics* 56, 1399.
- Chapman, S., Lindzen, R.S., 1970. *Atmospheric Tides*. D. Reidel, Hingham, MA.
- Coll, M.A.I., Forbes, J.M., 2002. Nonlinear interactions in the upper atmosphere: The $s = 1$ and $s = 3$ non-migrating

- semidiurnal tides. *Journal of Geophysical Research* 107, 1157.
- Dunkerton, T.J., 1997. The role of gravity waves in the quasi-biennial oscillation. *Journal of Geophysical Research* 102, 26053.
- Forbes, J.M., 1995. Tidal and planetary waves. *Geophysical Monograph* 87, 67.
- Forbes, J.M., Garrett, H.B., 1978. Thermal excitation of atmospheric tides due to insolation absorption by O₃ and H₂O. *Geophysical Research Letters* 5, 1013.
- Forbes, J.M., Makarov, N.A., Portnyagin, Y.I., 1995. First results from the meteor radar at South Pole: A large 12-hour oscillation with zonal wavenumber one. *Geophysical Research Letters* 22, 3247.
- Forbes, J.M., Hagan, M.E., Miyahara, S., Miyoshi, Y., Zhang, X., 2003a. Diurnal nonmigrating tides in the tropical lower thermosphere. *Earth Planets and Space* 55, 419.
- Forbes, J.M., Zhang, X., Talaat, E.R., Wand, W., 2003b. Nonmigrating diurnal tides in the thermosphere. *Journal of Geophysical Research* 108 (A1), SIA-7.
- Fritts, D.C., 1984. Gravity wave saturation in the middle atmosphere: A review of theory and observations. *Reviews of Geophysics and Space Physics* 22, 275.
- Fritts, D.C., 1995a. Gravity wave-tidal interactions in the middle atmosphere: observations and theory. *Geophysical Monograph* 87, 89.
- Fritts, D.C., 1995b. Gravity wave forcing and effects in the mesosphere and lower thermosphere. *Geophysical Monograph* 87, 121.
- Geller, M.A., Yudin, V.A., Khattatov, B.V., Hagan, M.E., 1997. Modeling the diurnal tide with dissipation derived from UARS/HRDI measurements. *Annales Geophysicae* 15, 1198.
- Hagan, M.E., Forbes, J.M., 2003. Migrating and nonmigrating semidiurnal tides in the upper atmosphere excited by tropospheric latent heat release. *Journal of Geophysical Research* 108 (A2), SIA-6.
- Hagan, M.E., Roble, R.G., 2001. Modeling diurnal tidal variability with the National Center for Atmospheric Research thermosphere-ionosphere-mesosphere-electrodynamics general circulation model. *Journal of Geophysical Research* 106, 24,869–24,882.
- Hagan, M.E., Chang, J.L., Avery, S.K., 1997. Global-scale wave model estimates of non-migrating tidal effects. *Journal of Geophysical Research* 102, 163493.
- Hays, P.B., et al., 1993. The high-resolution Doppler imager on the Upper Atmosphere Research Satellite. *Journal of Geophysical Research* 98, 10,713.
- Hays, P.B., Wu, D.L., the HRDI science team, 1994. Observations of the diurnal tide from space. *Journal of Atmospheric Science* 51, 3077.
- Held, I.M., Hou, A.Y., 1980. Nonlinear axially symmetric circulation in a near inviscid atmosphere. *Journal of Atmospheric Science* 37, 515.
- Hines, C.O., 1991a. The saturation of gravity waves in the middle atmosphere. Part I: Critique of linear instability theory. *Journal of Atmospheric Science* 48, 1348.
- Hines, C.O., 1991b. The saturation of gravity waves in the middle atmosphere. Part II: Development of Doppler spread theory. *Journal of Atmospheric Science* 48, 1360.
- Hines, C.O., 1997a. Doppler-spread parameterization of gravity-wave momentum deposition in the middle atmosphere, 1, basic formulation. *Journal of Atmospheric and Terrestrial Physics* 59, 371.
- Hines, C.O., 1997b. Doppler-spread parameterization of gravity-wave momentum deposition in the middle atmosphere, 2, broad and quasi monochromatic spectra, and implementation. *Journal of Atmospheric and Terrestrial Physics* 59, 387.
- Hines, C.O., 2001. Theory of the Eulerian tail in the spectra of atmospheric and oceanic internal gravity waves. *Journal of Fluid Mechanics* 448, 289.
- Hines, C.O., 2002. Nonlinearities and linearities in internal gravity waves of the atmosphere and the oceans. *Geophysical and Astrophysical Fluid Dynamics* 96, 1.
- Huang, F.T., Reber, C.A., 2003. Seasonal behavior of the semidiurnal and diurnal tides, and mean flows at 95 km, based on measurements from the High Resolution Doppler Imager (HRDI) on the Upper Atmosphere Research Satellite (UARS). *Journal of Geophysical Research* 108 (D12), 4360.
- Huang, F.T., Reber, C.A., 2004. Nonmigrating semidiurnal and diurnal tides at 95 km based on wind measurements from the High Resolution Doppler Imager (HRDI) on UARS. *Journal of Geophysical Research* 109, D10110.
- Jacobi, C., et al., 1999. Mesopause region semidiurnal tide over Europe as seen from ground-based wind measurements. *Advances in Space Research* 24, 1545.
- Lieberman, R., 1991. Non-migrating diurnal tides in the equatorial middle atmosphere. *Journal of Atmospheric Science* 48, 1112.
- Lindzen, R.S., 1981. Turbulence and stress due to gravity wave and tidal breakdown. *Journal of Geophysical Research* 86, 9707.
- Lindzen, R.S., Hou, A.Y., 1988. Hadley circulations for zonally averaged heating centered off the equator. *Journal of Atmospheric Science* 45, 4073.
- Manson, A.H., Meek, C.E., Teitelbaum, H., Vial, F., Schminder, R., Kuerschner, D., Smith, M.J., Fraser, G.J., Clark, R.R., 1989. Climatology of semi-diurnal and diurnal tides in the middle atmosphere (70–110 km) at middle latitudes (40–55°). *Journal of Atmospheric and Terrestrial Physics* 51, 579.
- Manson, A.H., Luo, Y., Meek, C., 2002. Global distribution of diurnal and semi-diurnal tides: observations from HRDI-UARS of the MLT region. *Annales Geophysicae* 20, 1877.
- Manzini, E., McFarlane, N.A., McLandress, C., 1997. Impact of the Doppler spread parameterization the simulation of the middle atmosphere circulation using the MA/ECHAM4 general circulation model. *Journal of Geophysical Research* 102, 25,751.
- Mayr, H.G., Mengel, J.G., Hines, C.O., Chan, K.L., Arnold, N.F., Reddy, C.A., Porter, H.S., 1997. The gravity wave Doppler spread theory applied in a numerical spectral model of the middle atmosphere, 1, Model and global scale seasonal variations. *Journal of Geophysical Research* 102, 26077.
- Mayr, H.G., Mengel, J.G., Chan, K.L., Porter, H.S., 2001a. Mesosphere dynamics with gravity wave forcing: Part I, Diurnal and semidiurnal tides. *Journal of Atmospheric and Terrestrial Physics* 63, 1851.

- Mayr, H.G., Mengel, J.G., Chan, K.L., Porter, H.S., 2001b. Mesosphere dynamics with gravity wave forcing: Part II, planetary waves. *Journal of Atmospheric and Terrestrial Physics* 63, 1865.
- Mayr, H.G., Mengel, J.G., Talaat, E.R., Porter, H.S., Chan, K.L., 2003. Non-migrating diurnal tides generated with planetary waves in the mesosphere. *Geophysical Research Letters* 30, 1832.
- Mayr, H.G., Mengel, J.G., Talaat, E.R., Porter, H.S., Chan, K.L., 2004a. Modeling study of mesospheric planetary waves: Genesis and characteristics. *Annales Geophysicae* 22, 1885.
- Mayr, H.G., Mengel, J.G., Talaat, E.R., Porter, H.S., Chan, K.L., 2004b. Properties of internal planetary-scale inertio gravity waves in the mesosphere. *Annales Geophysicae* 22, 3421.
- Mayr, H.G., Mengel, J.G., Talaat, E.R., Porter, H.S., Chan, K.L., 2005. Mesospheric non-migrating tides generated with planetary waves: II. Influence of gravity waves. *Journal of Atmospheric Solar-Terrestrial Physics*, in press.
- McLandress, C., Shepherd, G.G., Solheim, B.H., 1996. Satellite observations of thermospheric tides: Results from the Wind Imaging Interferometer on UARS. *Journal of Geophysical Research* 101, 4093.
- Mengel, J.G., Mayr, H.G., Chan, K.L., Hines, C.O., Reddy, C.A., Arnold, N.F., Porter, H.S., 1995. Equatorial oscillations in the middle atmosphere generated by small-scale gravity waves. *Geophysical Research Letters* 22, 3027.
- Miyahara, S., Miyoshi, Y., 1997. Migrating and nonmigrating atmospheric tides simulated by a middle atmosphere general circulation model. *Advances in Space Research* 20, 1201.
- Miyahara, S., Toshida, Y., Miyoshi, Y., 1993. Dynamical coupling between the lower and upper atmosphere by tides and gravity waves. *Journal of Atmospheric and Terrestrial Physics* 55, 1039.
- Miyahara, S., Miyoshi, Y., Yamashita, K., 1999. Variations of migrating and non-migrating atmospheric tides simulated by a middle atmosphere general circulation model. *Advances in Space Research* 24, 1549–1558.
- Oberheide, J., Hagan, M.E., Roble, R.G., Offermann, D., 2002. Source of nonmigrating tides in the tropical middle atmosphere. *Journal of Geophysical Research* 107 (D21), ACL-6.
- Pancheva, D., et al., 2002. Global-scale tidal variability during the PSMOS campaign for June–August 1999: interaction with planetary waves. *Journal of Atmospheric and Terrestrial Physics* 64, 1865.
- Plumb, R.A., 1983. Baroclinic instability of the summer mesosphere: A mechanism for the quasi-2-day wave? *Journal of Atmospheric Science* 40, 262.
- Plumb, R.A., Hou, A.Y., 1992. The response of a zonally symmetric atmosphere to subtropical thermal forcing: Threshold behavior. *Journal of Atmospheric Science* 49, 1790.
- Shepherd, G.G., et al., 1993. WINDII, the Wind Imager Interferometer on the Upper Atmosphere Research Satellite. *Journal of Geophysical Research* 98 (10), 7725.
- Strobel, D.F., 1978. Parameterization of atmospheric heating rate from 15 to 120 km due to O₂ and O₃ absorption of solar radiation. *Journal of Geophysical Research* 83, 7963.
- Talaat, E.R., Lieberman, R., 1999. Non-migrating diurnal tides in mesospheric and lower thermospheric winds and temperatures. *Journal of Atmospheric Science* 56, 4073.
- Teitelbaum, H., Vial, F., 1991. On tidal variability induced by nonlinear interaction with planetary waves. *Journal of Geophysical Research* 96, 14,169–14,178.
- Vincent, R.A., Tsuda, T., Kato, S., 1989. Asymmetries in mesospheric tidal structure. *Journal of Atmospheric and Terrestrial Physics* 51, 609.
- Volland, H., 1988. *Atmospheric Tidal and Planetary Waves*. Kluwer Academic Publishers, Boston, MA.
- Walterscheid, R.L., Sivjee, G.G., Schubert, G., Hamwey, R.M., 1986. Large amplitude semidiurnal temperature variations in the polar mesopause: evidence of pseudotide. *Nature* 324.
- Wehrbein, W.M., Leovy, C.B., 1982. An accurate radiative heating and cooling algorithm for use in a dynamical model of the middle atmosphere. *Journal of Atmospheric Science* 39, 1532.
- Yudin, V.A., Khattatov, B.V., Geller, M.A., et al., 1997. Thermal tides and studies to tune the mechanistic tidal model using UARS observations. *Annales Geophysicae* 15, 1205.
- Zhu, X., 1989. Radiative cooling calculated by random bans models with S-1-beta tailed distribution. *Journal of Atmospheric Science* 46, 511.